



# Numerical Modeling of Debris Flows: A Conceptual Assessment

# 5

Richard M. Iverson and David L. George

## Abstract

Real-world hazard evaluation poses many challenges for the development and application of numerical models of debris flows. In this chapter we provide a conceptual overview of physically based, depth-averaged models designed to simulate debris-flow motion across three-dimensional terrain. When judiciously formulated and applied, these models can provide useful information about anticipated depths, speeds, and extents of debris-flow inundation as well as debris interactions with structures such as levees and dams. Depth-averaged debris-flow models can differ significantly from one another, however. Some of the greatest differences result from simulation of one-phase versus two-phase flow, use of parsimonious versus information-intensive initial and boundary conditions, use of tuning coefficients versus physically measureable parameters, application of dissimilar numerical solution techniques, and variations in computational speed and model accessibility. This overview

first addresses these and related attributes of depth-averaged debris-flow models. It then describes model testing and application to hazard evaluation, with a focus on our own model, D-Claw. The overview concludes with a discussion of outstanding challenges for development of improved debris-flow models and suggestions for prospective model users.

## 5.1 Introduction

This chapter assesses the state of practical, physically based debris-flow modeling. By “practical” we mean modeling that addresses real-world questions about the anticipated speeds, depths, and extents of inundation caused by debris flows moving across three-dimensional terrain, including terrain that has been modified by construction of levees, roads, buildings, and dams. By “physically based” we mean modeling that obeys physical conservation laws as closely as possible and that minimizes use of adjustable coefficients. The chapter does not include a comprehensive literature review or detailed descriptions of individual debris-flow models, which number in the dozens (e.g., Trujillo-Vela et al., 2022). Instead, it focuses on concepts and principles that are relevant across a spectrum of models and on features that distinguish models from one another.

R. M. Iverson (✉) · D. L. George  
U.S. Geological Survey, 1300 SE Cardinal Ct.,  
Vancouver, WA 98683, USA  
e-mail: [riverson@usgs.gov](mailto:riverson@usgs.gov)

D. L. George  
e-mail: [dgeorge@usgs.gov](mailto:dgeorge@usgs.gov)

The chief goal of the chapter is to provide a nonmathematical summary of information that may be useful to scientists and engineers who are not model developers themselves but are knowledgeable about debris flows and wish to use numerical models to simulate them. Such model users are effectively consumers of products created or marketed by others. The chapter aims to equip such model users with a healthy skepticism that characterizes consumers who are well-informed.

We are model developers ourselves, but we are also model skeptics. Our skepticism comes from studying numerous models, from recognizing our own limitations in model development, and from humility born of long experience with the natural complexities of debris flows. Unlike geological phenomena that are hidden by the veils of deep Earth or deep time, debris flows occur routinely and are readily observed. It consequently can be easy to see when predictions of debris-flow models are wrong. However, some prediction errors result from fundamental model shortcomings, whereas others result from uncertainties about debris properties, volumes, or initial states. Thus, some types of erroneous predictions should increase the skepticism of model users, whereas others should boost users' confidence by quantifying the effects of uncertainties that are inherently part of the natural world (e.g., Barnhart et al., 2021b).

Our overview first explains how the diversity of depth-averaged debris-flow models reflects differences in model conceptualization, formulation, idealization, parameterization, testability, and accessibility. It then describes examples of model testing and application to hazard evaluation, with a focus on our own model, D-Claw. Model testing entails comparing model predictions with detailed measurements made in a laboratory setting, and also with less-detailed but highly relevant field measurements of phenomena such as flow speeds, depths, runup heights, and inundation patterns. The overview concludes with a discussion of outstanding challenges for development of improved debris-flow models and with suggestions for prospective model users.

## 5.2 Physical Characteristics of Debris Flows

The design of useful debris-flow models should account for the fact that debris flows encompass a range of Earth-surface flow phenomena intermediate in character between rock avalanches and sediment-laden water floods. Like rock avalanches, debris flows typically begin on slopes steeper than  $25^\circ$  and have definite starting and ending points in space and time, but like water floods, debris flows can travel great distances across low-relief terrain—more than 100 km in the case of Earth's largest volcanic debris flows (Vallance & Iverson, 2015). The observation that debris flows share some attributes with both rock avalanches and water floods has influenced the development of many debris-flow models, some of which are rooted in rock-avalanche modeling, and some of which are rooted in flood-wave modeling (McDougall, 2017; Rickenmann et al., 2006; Trujillo-Vela et al., 2022).

Debris flows differ from either rock avalanches or water floods, however, and these differences have important implications for model formulation and application. Most conspicuously, debris flows contain roughly equal volumes of liquid water and solid grains. Whereas momentum transfer and energy dissipation are dominated by solid grain forces in rock avalanches and by fluid dynamical forces in water floods, mechanical interactions between grains and fluid have large effects on the physics of debris flows. Moreover, solid–fluid interactions evolve as debris flows transition from static initial states to rapidly flowing states and then transition again to form nearly rigid deposits. The prominent role that solid–fluid interactions play in causing these transitions and mediating flow resistance is a key feature of debris flows (Iverson, 1997, 2003a).

Another key feature of debris flows is the presence of grains with diverse shapes, sizes, and compositions (Hungri et al., 2001, 2014; Varnes, 1978). This trait distinguishes debris flows from phenomena investigated in

laboratory or theoretical studies that focus on flows of identical solid spheres immersed in liquid (e.g., Berzi et al., 2010). Such investigations can have great scientific value, but they have limited relevance for practical modeling of debris flows in which grains commonly range from clay-sized particles to boulders exceeding 1 m in diameter. In some cases debris flows also carry a significant freight of woody debris, including large logs (Fig. 5.1).

The diversity of grains in debris flows permits a great variety of grain arrangements, which affect debris bulk density and dilatancy (i.e., shear-induced volumetric dilation/contraction of the granular fraction of deforming debris). Debris bulk density can also vary in response to changes in debris agitation, grain-size segregation, debris dilution during mixing with water bodies, and erosion or sedimentation. Consequently, from a modeling perspective, debris mixtures effectively behave as compressible materials with bulk densities that commonly vary from about 1600 to 2400 kg/m<sup>3</sup>—even though the individual solid and liquid constituents of debris are nearly incompressible (Iverson, 1997; Iverson et al., 2010).

Changes in debris bulk density are generally accompanied by changes in intergranular fluid pressure that affects intergranular friction and bulk flow resistance (George & Iverson, 2014; Iverson, 1997; Iverson & George, 2014; Iverson et al., 2010). The diversity of grain sizes in debris flows enhances this effect because it

reduces the hydraulic permeability of debris by increasing solid–fluid drag forces that result from fluid moving with respect to grains on a local scale (Iverson, 1997). On a continuum scale encompassing thousands of grains and their adjacent fluid, high intergranular fluid pressures that develop during contractive debris deformation can lead to partial or complete debris liquefaction. The presence of more than several weight percent silt- and clay-sized grains helps perpetuate liquefaction and thereby increases debris-flow mobility (Iverson et al., 2010). In contrast, the presence of silt- and clay-sized sediment can reduce the mobility of miniature, laboratory-scale debris flows because it provides some cohesive yield strength. Mobility reduction caused by cohesive strength is a scale-dependent phenomenon, however, and it typically has little importance in natural debris flows with volumes ranging from thousands to billions of cubic meters (Iverson, 2003a, 2015).

Conspicuous grain-size segregation occurs in many debris flows, and it can significantly affect macroscopic flow dynamics and the formation of deposits (Iverson et al., 2010; Major & Iverson, 1999). One consequence of size segregation is development of coarse-grained, high-friction surge fronts that impede the motion of finer-grained trailing debris in which liquefaction is persistent (Iverson et al., 2010; Sharp & Nobles, 1953). Typically, this liquefied sediment-rich debris is trailed by more-dilute debris that in turn is trailed by muddy water (Pierson,



**Fig. 5.1** Boulders, finer sediment, and wood fragments deposited by a rain-triggered debris flow that descended the Eliot Branch and Middle Fork Hood River, Oregon, USA, on 7 November 2006. The debris flow began roughly 8 km distant and 1 km higher in elevation than

this deposition site just upstream of the confluence of the Eliot Branch and Middle Fork Hood River. It was sourced primarily from landslides on lateral moraines of Eliot Glacier on snow-clad Mount Hood in the background. Photo courtesy of Darryl Lloyd

1986). Another consequence of grain-size segregation is the development of coarse-grained lateral levees that commonly form where debris flows begin to escape or overtop constricted channels (Johnson et al., 2012). These natural levees can channelize ensuing flow and thereby increase runout distance by focusing debris-flow momentum downstream (Fig. 5.2). Alternatively, levees can be breached or overtopped by successive debris-flow surges, leading to flow avulsion and redirection of downstream inundation (de Haas et al., 2018). Thus, development of multiple surge fronts and levees during individual debris-flow events can strongly influence the distribution of associated hazards.

Entrainment of debris along flow paths is another phenomenon that influences debris-flow dynamics and hazards. Entrainment is typically concentrated in the steep, narrow, upper reaches of debris-flow paths, particularly in areas where channels slope at angles greater than about  $10^\circ$  (Hung et al., 2005). Entrainment can occur through scour of bed material, especially if the bed material is wet and loose enough to weaken as a result of excess pore-fluid pressure generated when it is suddenly overrun (Iverson et al., 2011; McCoy et al., 2012; Reid et al., 2011). It



**Fig. 5.2** Boulder-rich lateral levee deposited by the same debris flow that emplaced the deposits pictured in Fig. 5.1. The levee formed approximately 7 km downstream from the site shown in Fig. 5.1, and it focused debris-flow momentum into the channel of the Middle Fork Hood River, visible on the right side of the photo. Largest boulders in the levee were  $>2$  m in diameter

can also occur by undermining of steep channel banks, resulting in sloughing of debris onto the surface of passing debris flows. In some cases the majority of a debris flow's final volume results from entrainment that occurs along its path, greatly increasing the scope of impacts in debris-flow runout zones (Breien et al., 2008; Hung et al., 2005; Pierson et al., 1990).

Finally, an important feature of most debris flows is that they are “shallow,” meaning that their typical thicknesses are much less than their typical planimetric dimensions—commonly by a factor of 10 or more (Fig. 5.3). Most river floods, storm surges, and tsunamis inundating coastlines also satisfy this shallowness criterion. Debris-flow modeling consequently has exploited a large body of mathematical and computational knowledge developed to simulate shallow-water flow phenomena (e.g., Berger et al., 2011; Vreugdenhil, 1994). Nevertheless, as summarized in the preceding paragraphs, debris flows have many distinctive attributes, and simple adjustments of flow resistance coefficients in shallow-water flow models are unlikely to yield debris-flow models that reliably predict quantities of practical importance such as flow speeds, depths, and inundation patterns.

### 5.3 Depth-Averaged Conservation Equations

The mathematical core of nearly all practical, physically based debris-flow models consists of partial differential equations that represent depth-averaged continuum-mechanical mass and momentum conservation laws for flows that are “shallow” as illustrated in Fig. 5.3 (e.g., Iverson & George, 2014). The same is true of most physically based models of high-speed landslides that don't qualify as debris flows (e.g., McDougall, 2017). However, a potential source of confusion is that we categorize depth-averaged models for motion across three-dimensional terrain as 2-D models, whereas McDougall (2017) categorized them as 3-D models. We reserve the term “3-D” for models that do not use depth averaging.

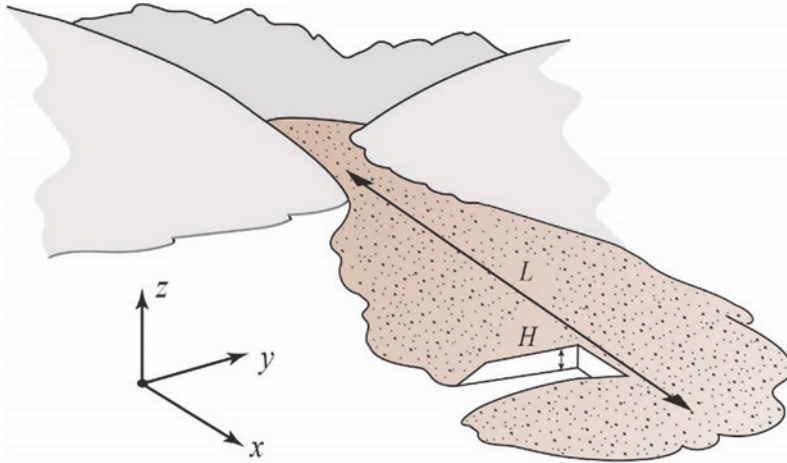


**Fig. 5.3** Debris flows satisfy a “shallowness” criterion if their characteristic thickness  $H$  in the  $z$  direction is much less than their characteristic extent  $L$  in the  $x$  and  $y$  directions, as illustrated in this schematic (adapted from Iverson, 2005)

Whereas 3-D models calculate evolving momentum fluxes in three coordinate directions, most depth-averaged models assume that momentum fluxes normal to the bed can be neglected—implying that basal normal stresses balance the static weight of overlying debris. Iverson (2005) provided a quantitative assessment of this assumption and of ways that it can be relaxed. Although the assumption of static basal normal stress might seem highly restrictive, experience with depth-averaged models of diverse phenomena ranging from tsunamis and floods to granular avalanches has shown that these models commonly yield suitable practical predictions even for flows in which the assumption is locally or transiently violated (e.g., George, 2010; Gray et al., 2003; LeVeque et al., 2011).

Depth-averaged debris-flow models also generally assume that depth-dependent variations in downstream momentum are negligible. As in shallow-water flow models, corrections for the effects of these variations can be made by introducing momentum-distribution coefficients (e.g., Vreugdenhil, 1994). However, values of the distribution coefficients depend on the shape of flow velocity and density profiles, which are poorly constrained for debris flows. Most depth-averaged debris-flow models consequently

exclude the coefficients as an unwarranted complication. They instead assume that downstream debris-flow momentum can be approximated as uniform at all depths.

Depth-averaged conservation equations are derived by integrating 3-D conservation equations through the debris-flow thickness in the coordinate direction we denote with  $z$  in Fig. 5.3 (Iverson, 2005). However, the direction of  $z$  is not the same in every model. Terrain-fitted curvilinear coordinates with  $z$  rotated so that it is everywhere normal to the bed are the most rigorous coordinates from a mathematical standpoint, and they facilitate accounting for the effect of centripetal accelerations on basal stresses (Gray et al., 1999; Pudasaini et al., 2005; Savage & Hutter, 1991). However, curvilinear coordinates can be difficult to employ in numerical simulations of flow across rugged 3-D terrain, in part because adjacent computational cells can have sharp differences in bed-normal  $z$  directions, potentially resulting in conflicting definitions of flow depths (Fig. 5.4). Moreover, if the bed geometry changes significantly owing to erosion or deposition, curvilinear coordinates fitted to the original terrain lose at least some of their relevance. Use of Earth-centered Cartesian coordinates with  $z$  uniformly vertical is simpler, but it requires care in calculation of momentum

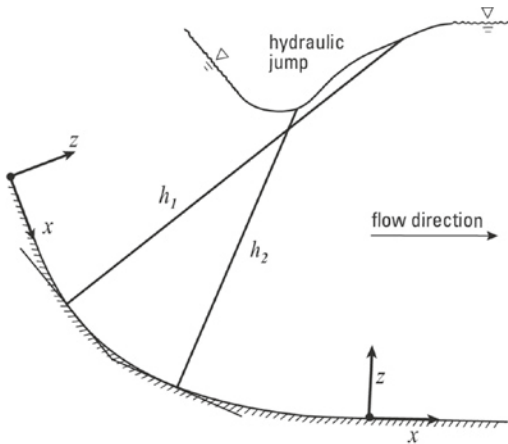


**Fig. 5.4** Schematic vertical cross section illustrating a debris flow moving across variably sloping, discretized bed topography with terrain-fitted coordinates. As the flow passes through a hydraulic jump, the flow thickness  $h$  in the  $z$  direction is incorrectly represented with respect to discretized bed topography, because the flow depth  $h_1$  (upstream) is larger than  $h_2$  (downstream). Use of Earth-centered Cartesian coordinates with  $z$  vertical everywhere eliminates this issue

fluxes and basal stresses, because the orientation of sloping beds is not normal to a vertical  $z$  coordinate (Denlinger & Iverson, 2004; Iverson, 2005; Iverson & George, 2019a).

In all depth-averaged debris-flow models the fundamental conserved quantities (mass and linear momentum) are expressed per unit area in

the  $x$ - $y$  plane, which is normal to  $z$  (Fig. 5.3). For example, in the notation of Iverson (2005) and many others, the  $x$ -direction momentum component per unit area is expressed as  $\rho uh$ , where  $\rho$  is the debris bulk density,  $u$  is the  $x$  component of velocity, and  $h$  is the debris thickness in the  $z$  direction (Table 5.1). Similarly, the debris mass per unit area is expressed as  $\rho h$ . In single-phase debris-flow models that assume  $\rho$  is constant (described further in the next section),  $\rho$  is typically cancelled from the conservation equations so that it does not explicitly appear.

Use of depth-averaged rather than 3-D conservation equations aids development of efficient numerical solution techniques, in part because free-surface and basal boundary conditions are embedded in the equations during the depth-integration procedure (Iverson, 2005; Iverson & Ouyang, 2015). This feature eliminates the need to separately resolve the evolving boundary positions as computational solutions proceed. However, during depth integration it can be challenging to properly incorporate the effects of a basal boundary where erosion or deposition occurs because fluxes of mass and momentum across an irregular, evolving surface are involved. The problem can be addressed rigorously by adopting a two-layer perspective in which the debris flow constitutes the upper layer and the bed constitutes the lower layer, and then

**Table 5.1** Definitions of variables commonly used in some depth-averaged debris-flow models

Typical symbols	Definitions
<i>Independent variables</i>	
$x, y$	Planimetric spatial coordinates
$z$	Vertical or slope-normal coordinate
$t$	Time coordinate
<i>Dependent variables that evolve as functions of <math>x, y</math> and <math>t</math></i>	
$u, v$	Flow velocity components in $x$ and $y$ directions <sup>a</sup>
$h$	Flow thickness in $z$ direction <sup>a</sup>
$\rho$	Debris bulk density <sup>b</sup>
$m$	Debris solid volume fraction <sup>b</sup>
$P_{bed}$	Basal pore-fluid pressure

<sup>a</sup>Two-phase models typically include separate values of  $u$ ,  $v$ , and  $h$  for each phase

<sup>b</sup>Use of both  $\rho$  and  $m$  as variables can be redundant because  $\rho = \rho_s m + \rho_f (1 - m)$  applies and the solid grain density  $\rho_s$  and intergranular fluid density  $\rho_f$  are generally treated as constants

enforcing mass and momentum conservation in each layer as well as in the two-layer system as a whole (Iverson & Ouyang, 2015). Han et al. (2015) implemented a simplified form of this approach (cf. Iverson, 2012), but to our knowledge a more complete implementation has not been utilized in model applications to practical hazard assessment.

Finally, we note that depth-averaged numerical models are most likely to be sound if details of the depth-integration procedure have been presented in publications that can be scrutinized. In our experience, model formulations that skip steps in the depth-integration procedure can lead to spurious equations with hidden assumptions or even to equations that violate physical conservation laws. No aspect of debris-flow modeling is more important than satisfying physical conservation laws, which provide the strongest block in the foundation of debris-flow science.

---

#### 5.4 One-Phase Versus Two-Phase Models

The simplest depth-averaged models idealize debris flows as one-phase materials with fixed bulk densities. These models include three conservation equations, one expressing mass conservation and two expressing conservation of orthogonal components of either bed-parallel or horizontal linear momentum (e.g., McDougall & Hungr, 2004; Rickenmann et al., 2006). The three equations generally differ from the standard shallow-water equations only in their definitions of flow resistance and longitudinal stress coefficients. Their similarity to the shallow-water equations has significant advantages from a mathematical and computational standpoint because the shallow-water equations have a long history of theoretical analysis, numerical solution, and practical application (e.g., Berger et al., 2011; Vreugdenhil, 1994). However, one-phase debris-flow models omit a central feature of debris-flow behavior: natural evolution of flow resistance that results from evolving interactions of solid and fluid constituents during evolution of debris velocity and bulk density.

This evolution indicates that flow resistance is an emergent property that coevolves with flow dynamics (Iverson, 2003a), implying that it is inappropriate to specify evolving flow resistance a priori.

Models that treat debris flows as two-phase materials with evolving bulk densities, solid–fluid interactions, and flow resistance typically include four to six conservation equations. One of these equations expresses conservation of solid mass and another expresses conservation of either fluid mass or conservation of mass for the two-phase mixture as a whole. The other conservation equations express either orthogonal momentum components of separate but interacting solid and fluid constituents (e.g., Bouchut et al., 2016; Meyrat et al., 2022; Pitman & Le, 2005; Pudasaini, 2012) or orthogonal momentum components of a two-phase mixture in which the solid and fluid volume fractions evolve as the solid and fluid constituents interact (Iverson & George, 2014; Kowalski & McElwaine, 2013). The conceptual underpinnings of these two approaches are similar but differ in one important respect. An approach that considers distinct solid and fluid phases allows for the possibility of complete separation of the two phases into bodies composed entirely of fluid or entirely of solid grains, whereas an approach that considers a two-phase mixture assumes that some amalgamation of grains and fluid is always present—albeit with grain or fluid concentrations that might become very small in some circumstances.

A fundamental issue in the formulation of all two-phase debris-flow models concerns definition of the fluid phase. A rationale provided by Iverson (1997) is that the fluid phase includes small grains that can remain suspended by purely hydrodynamic forces—without need of grain interaction forces—for the duration of a debris flow. These suspended small particles increase the effective fluid viscosity relative to the viscosity of pure water, and in sufficiently high concentrations they can confer some fluid-phase yield strength. Typically, these small particles are clay-sized and silt-sized (<0.0625 mm), whereas larger particles are treated as part of the

granular phase. Muddy water that drains from the margins of fresh debris-flow deposits provides evidence that silt- and clay-sized particles can remain in suspension even after debris-flow motion ceases (e.g., Logan et al., 2007).

The use of more than three conservation equations in two-phase and two-phase mixture models makes their mathematical and computational structure more complicated than that of one-phase models. However, the use of additional conservation equations simplifies two-phase and two-phase mixture models from a physical standpoint because it reduces the breadth of assumptions used in deriving the equations and it sharpens the definitions of model parameters. The total number of differential equations in any debris-flow model must of course equal the total number of dependent variables in the model. A basic tenet of mathematical physics, applicable in debris-flow modeling, is that predicting the values of increasing numbers of dependent variables enables increasingly diverse and stringent model tests. Models that can successfully predict the values of the largest number of dependent variables simultaneously are the most likely to be physically correct (Iverson, 2003b).

---

## 5.5 Ancillary Equations, Variables, Parameters, and Tuning Coefficients

Depth-averaged debris-flow models generally include ancillary equations that supplement the core conservation equations. For example, our D-Claw model includes a differential equation describing evolution of basal pore-fluid pressure, which is derived and solved in conjunction with the conservation equations but does not express a physical conservation law (George & Iverson, 2014; Iverson & George, 2014, 2016). Other differential equations with similar relationships to conservation laws have been derived to describe phenomena such as grain-size segregation (Gray & Kokelaar, 2010) or granular temperature (a measure of kinetic energy associated with random grain motions in agitated

debris). Such ancillary equations account for evolution of dependent variables that is fully coupled to evolution of the basic dependent variables that appear in depth-averaged conservation laws (Table 5.1). A model's use of ancillary differential equations accounts for the fact that relationships among quantities that serve as dependent variables in the equations may evolve in a variety of ways, contingent on the evolution of all other dependent variables in the model and on the auxiliary conditions they satisfy (see Sect. 5.6).

The ancillary equations most commonly used in debris-flow models are not differential equations; instead, they are algebraic equations that prescribe relationships that do not evolve. Unlike use of a differential equation, use of an algebraic formula relating two or more quantities implies knowledge of an immutable relationship between the quantities, whereas use of a differential equation implies less omniscience. In debris-flow models algebraic formulas are typically used to specify various kinds of basal or internal flow resistance, solid–fluid drag forces, lateral stress transfer, basal erosion or sedimentation rates, or other energy-dissipating phenomena that are not easily characterized by using continuum conservation laws alone. In some cases authors identify these ancillary formulas as “rheologies” or even “laws,” but such labels are generally inappropriate. True rheological formulas—sometimes called constitutive equations—must satisfy strict mathematical and physical criteria and be cast in three-dimensional vector/tensor forms (e.g., Malvern, 1969). Few ancillary formulas used in depth-averaged debris-flow models satisfy these criteria.

Ancillary equations are commonly the place where most parameters and tuning coefficients are introduced in debris-flow models. Here we use “parameter” to describe model quantities that have a clear physical basis and are measurable outside the context of any model (Table 5.2). For example, debris friction angles, which are measurable in geotechnical tests and estimable from sediment angles of repose, qualify as physical parameters. The same is true of debris hydraulic permeabilities, which can be measured

**Table 5.2** Definitions of parameters and tuning coefficients commonly used in some depth-averaged debris-flow models

Typical symbols	Definitions
<i>Physical parameters</i>	
$\phi_{int}$	Internal friction angle of granular debris
$\phi_{bed}$	Basal friction angle of granular debris in contact with bed
$\rho_s$	Mass density of solid grains
$\rho_f$	Mass density of intergranular fluid
$\mu$	Viscosity of intergranular fluid
$k_0$	Debris hydraulic permeability in initial state
$\alpha_0$	Debris compressibility in initial state
$m_{crit}$	Debris critical-state solid volume fraction in initial state
<i>Tuning coefficients</i>	
$A$	Coefficient of basal flow resistance independent of flow velocity
$B$	Coefficient of basal flow resistance proportional to flow velocity
$C$	Coefficient of basal flow resistance proportional to flow velocity squared

in permeameter tests or slug tests, and of the viscosity of muddy intergranular water, which is readily measured using a standard benchtop viscometer.

In contrast to our definition of parameters, we define model tuning coefficients as quantities that are used to fit model results to observations of macroscopic debris-flow behavior but that lack clear links to independent physical measurements outside the context of any model. For example, some debris-flow models such as the well-known FLO-2D model use basal flow-resistance formulas similar to  $R = A + Bv + Cv^2 + \dots$ , where  $R$  is the total flow resistance,  $v$  is the magnitude of flow velocity, and  $A$ ,  $B$ , and  $C$  are tuning coefficients (Table 5.2). An equation of this form can provide a power-series representation of almost any functional dependence of  $R$  on  $v$ . Owing to this flexibility, tuning the values of  $A$ ,  $B$ , and  $C$  may yield appealing fits of model output to observations of debris-flow behavior. There is nothing fundamentally wrong with such a model tuning procedure, provided that its scientific basis and interpretation are not misrepresented. Some publications have stated that a coefficient analogous to  $A$  represents a combination of cohesive and frictional resistance, a coefficient proportional

to  $B$  represents viscous resistance, and a coefficient proportional to  $C$  represents resistance due to turbulence and/or gain inertia during shearing (e.g., O'Brien et al., 1993). If these descriptions were scientifically valid, then values of  $A$ ,  $B$ , and  $C$  could be readily interpreted and could be determined from experiments or estimated from field data that are wholly independent of any model. When  $A$ ,  $B$ , and  $C$  are used as tuning coefficients, however, that is not the case.

From a practical rather than scientific perspective, why does the difference between physical parameters and tuning coefficients matter? An important reason is that appropriate values of physical parameters are commonly constrained by a great body of accumulated knowledge that is independent of specific models but is potentially useful in all models. For example, few experienced debris-flow investigators would estimate that applicable values of the Coulomb friction angle  $\phi$  of the granular fraction of debris lie outside the range  $20^\circ \leq \phi \leq 50^\circ$ . Such a range constraint is applicable regardless of whether the debris of interest is part of a small alpine debris torrent or a great volcanic lahar. Indeed, applicability from one location to another—and from one model to another—is a great advantage that physical parameters hold over tuning

coefficients. If all debris-flow models used physically defined parameters rather than tuning coefficients, then debris-flow science and model-based hazard evaluation could advance more rapidly because comparisons between predictions of different models could be more direct (e.g., Barnhart et al., 2021b).

## 5.6 Initial and Boundary Conditions

Numerical solution of the system of partial differential equations in depth-averaged debris-flow models requires specification of appropriate initial and boundary conditions, collectively called auxiliary conditions. These conditions must satisfy physical constraints and must be ascertainable from a priori knowledge. Additionally, they must be posed in a manner consistent with the mathematical properties of the conservation equations themselves, which generally can be classified as hyperbolic. Mathematical properties of hyperbolic partial differential equations are beyond the scope of this chapter, but an overarching property is that

auxiliary conditions appropriate for various uses of the equations can differ greatly.

The boundary conditions for some debris-flow models can be easily and unequivocally specified because the domain boundaries can be placed arbitrarily far from any location where debris might originate or travel. At these distant boundary locations, values of all dependent variables can be set equal to zero for the duration of a simulation (Fig. 5.5). Use of this parsimonious boundary condition is standard when our own model, D-Claw, is applied to real-world problems (Barnhart et al., 2021a; George et al., 2017, 2022; Iverson & George, 2016), but not all debris-flow models are structured or implemented in this way. For example, some models require information-intensive specification of the depths and velocities (i.e., hydrographs) of incoming flows that enter upstream domain boundaries. Such differences in the type and scope of a priori information requirements reflect fundamental differences in the epistemological framework of the models, complicating the task of comparing the models' predictive value (Barnhart et al., 2021b).

If the goal is merely to fit model results to the outcome of a past debris-flow event, models

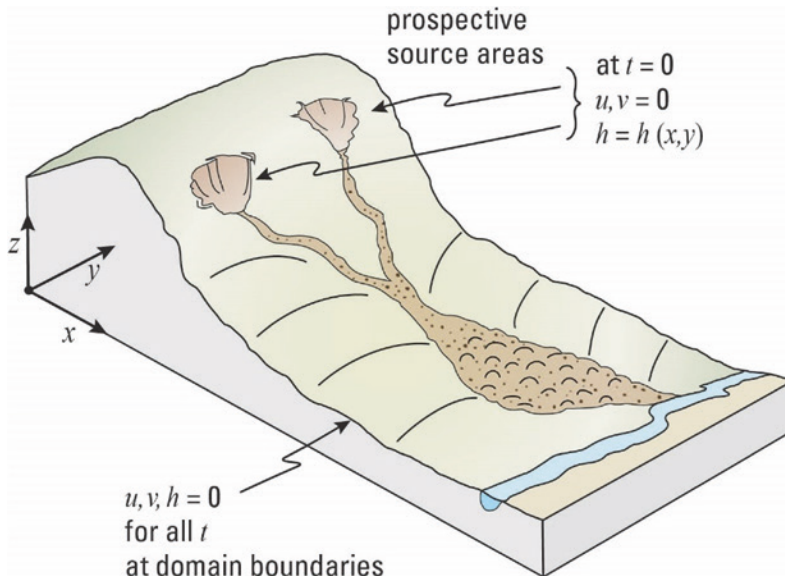


**Fig. 5.5** Schematic block diagram illustrating debris-flow paths that lie entirely within the boundaries of a rectangular computational domain. The dependent variables

$u$ ,  $v$ ,  $h$ , and independent variables  $x$ ,  $y$ ,  $z$ , and  $t$  are defined in Table 5.1. The initial and boundary values of  $u$ ,  $v$ , and  $h$ , as implemented in D-Claw, are shown in the figure

that use freely adjustable, information-intensive boundary information have a competitive advantage over those that use fixed, parsimonious boundary information because adjustable boundary information can be tailored to produce the desired model output. On the other hand, if the goal is to predict the behavior of future debris flows, the use of freely adjustable boundary information diminishes a model's value because it requires some omniscience by the model user who makes the adjustments. Parsimonious boundary conditions are consistent with unambiguous physical constraints and don't require such adjustments.

Initial conditions used in depth-averaged debris-flow models can be just as diverse as boundary conditions. However, regardless of the type of initial condition used, the volume of potentially mobilized debris has an overarching importance for anticipating debris-flow runout (Griswold & Iverson, 2008; Iverson et al., 1998; Reid et al., 2016) and simulating debris-flow motion (Barnhart et al., 2021b). Any model application that assumes or calculates a seriously flawed debris-flow volume cannot be

expected to yield good predictions of debris-flow speeds, depths, and inundation patterns. Estimation of future flow volumes and source locations is consequently an essential step in specifying initial conditions for all debris-flow models that are used to make predictions—and it is a step in which considerable uncertainties may be involved.

On the other hand, some physical certainties can be exploited in specifying initial conditions and flow volumes for debris-flow models. For example, the initial state of debris-flow material is unquestionably a state of static mechanical equilibrium with balanced driving and resisting forces. Static debris is initially poised on slopes or in channels and is ready to move under the influence of a physical perturbation such as rainfall that increases pore-water pressures in slopes and/or the discharge of water in channels. A small perturbation of such a statically balanced state is the initial condition typically used in D-Claw, for example (Fig. 5.6a). This initial condition is parsimonious because the statically balanced initial state satisfies unambiguous physical constraints.

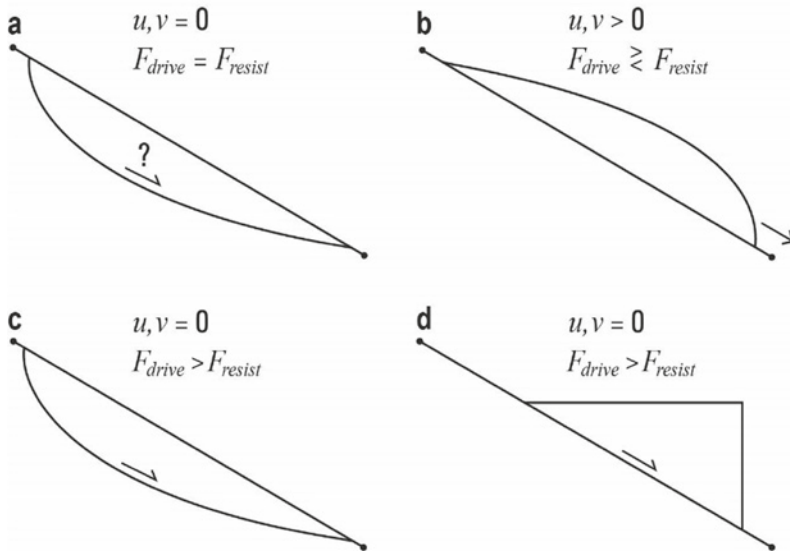


**Fig. 5.6** Schematic vertical cross-sectional views of initial conditions used in various debris-flow models. **a** Debris at rest satisfies a static equilibrium force balance with driving forces ( $F_{drive}$ ) equal to resisting forces ( $F_{resist}$ ). **b** Debris in motion may or may not satisfy an

equilibrium force balance. **c** Debris at rest does not satisfy a static equilibrium force balance, but motion is prohibited until a computer command is issued. **d** Debris at rest is constrained by an imaginary vertical dam that vanishes when a computer command is issued

Some other debris-flow models use information-intensive initial conditions in which a priori flow depths and velocities must be specified (Fig. 5.6b). This type of initial condition is commonly used in flood-wave modeling, but river floods differ fundamentally from debris flows because most rivers flow continually. Moreover, the flows of many rivers are gauged, providing data to constrain the flow depths and velocities that precede a flood. By contrast, specifying flow depths and velocities in advance of a debris flow requires considerable guesswork.

Still other debris-flow models use various forms of dam-break initial conditions. In these cases modelers specify a spatial distribution of static debris in prospective debris-flow source areas, but they do not require the debris to satisfy an initial state of static mechanical equilibrium in which gravitational driving forces are balanced by resisting forces (Fig. 5.6c). Instead, the simulated debris is artificially held in place by withholding a computer command. Issuing a command instantaneously places the debris in a far-from-equilibrium state in which driving forces greatly exceed resisting forces, mimicking the effect of an idealized, instantaneous dam break (Fig. 5.6d). This type of initial condition produces a “hot start” in which an abrupt conversion of potential energy to kinetic energy occurs during the onset of debris-flow motion (Iverson & George, 2019b). The abrupt energy conversion appears explicitly in analytical solutions of dam-break problems but it may be less obvious in graphs portraying the results of numerical simulations. Such hot-start initial conditions are convenient to use, but they involve an unphysical representation of the initial state of static debris. Indeed, detailed findings obtained using our D-Claw model show that instantaneous dam-break initial conditions yield inaccurate results even when simulating experimental debris flows that are abruptly released from a headgate at the top of the USGS debris-flow flume. Accurate simulations of these experimental debris flows require an accurate kinematic representation of the headgate opening style and rate (George & Iverson, 2014).

From a practical rather than scientific perspective, why does the difference between physical and unphysical auxiliary conditions matter? Perhaps the most important reason is that physical auxiliary conditions can be constrained by direct a priori observations of static debris on a landscape, whereas unphysical conditions cannot. Physical law requires that static mechanical equilibrium is satisfied by debris poised on slopes or in channels prior to the onset of debris-flow motion. Moreover, the volume and distribution of static debris that may be susceptible to motion can be inferred from topographic, geologic, and soils maps, supplemented by field observations, subsurface investigations, and geomechanical analysis. Such detailed information is not available in every circumstance, but obtaining such information is at least plausible. Accurately specifying future disequilibrium states of debris (i.e., states that do not satisfy mechanical equilibrium) is a more formidable task. Indeed, modern understanding of nonlinear dynamical systems indicates that it is fundamentally impossible to specify future disequilibrium states, because debris flows are nonlinear phenomena that may evolve in diverse ways contingent on initial conditions.

---

## 5.7 Base Topography Resolution and Numerical Discretization

Use of depth-averaged debris-flow models requires specification of base topography for areas where debris flows originate, travel, and come to rest. Moreover, if debris flows enter bodies of water such as lakes or rivers, specification of bathymetric data for lakebeds or riverbeds is required to define the basal surface and the ambient depth of water above the bed. Topographic and bathymetric base data commonly are available as digital elevation models (DEMs) that provide gridded elevations referenced to regularly spaced planimetric coordinates. If such data are unavailable, DEMs can be constructed by digitizing analog data such as topographic contours, although this type of DEM construction can be labor-intensive.

The resolution of DEM data is an important consideration in debris-flow modeling. A coarse DEM with 10 or 20 m horizontal resolution may be satisfactory for modeling great lahars (volcanic debris flows) involving hundreds of millions of cubic meters of debris and inundating 100 km<sup>2</sup> or more of low-relief terrain. On the other hand, DEMs with sub-meter resolution (typically acquired using Lidar, structure-from-motion digital photography, or some analogous technology) may be necessary for modeling debris flows that involve only thousands of cubic meters of material descending mountain-front channels and alluvial fans. In other cases, hybrid resolutions may be warranted, because relatively coarse DEMs may be satisfactory for some parts of debris-flow paths but high-resolution DEMs may be required to portray accurately some high-value/high-consequence features such as buildings, levees, or dams in debris-flow runout zones. However, not all numerical methods are well-suited for solving depth-averaged conservation equations for flow across topographic surfaces portrayed with variable resolutions (see Sect. 5.8 that follows).

Use of a computational grid resolution that corresponds to the maximum available DEM resolution throughout any domain might seem desirable, but in many cases it isn't practical because it comes at the expense of greatly increased computation time. For 2-D depth-averaged models, the number of computational grid cells in the domain scales with the square of the lineal spatial resolution. However, computation time typically scales with the cube of the lineal resolution, because fine spatial discretization requires commensurately fine temporal discretization in order to satisfy the Courant–Friedrichs–Lewy condition and thereby permit numerical accuracy and stability. Thus, doubling the lineal topographic resolution by replacing one square grid cell with four square grid cells generally implies that the computation time will increase about eightfold. Moreover, a large-scale computation requiring 1 day of runtime on a 10 m grid would typically require about 1000 days of runtime on a 1 m grid. Considerable care is consequently required

in selecting the numerical grid resolution for a given problem. Furthermore, the optimal grid resolution generally varies throughout the course of a simulation, implying that fixed or static computational grids are suboptimal.

The incorporation of DEM data into a model's numerical discretization can be accomplished in a variety of ways. The simplest approach is to utilize fixed computational grids that align with gridded DEM data. However, this approach has disadvantages such as the requirement of a uniform resolution throughout a rectangular domain within which a debris flow typically inundates only a small fraction of the grid cells (e.g., Fig. 5.5). An alternative is to construct non-uniform computational meshes that conform to topographic features through interpolation of the gridded DEM data. The meshes may be unstructured (for example, triangular irregular networks (TINs)) or based on terrain-fitted curvilinear coordinates. While these approaches can provide improvements in terms of computational efficiency or numerical accuracy in some cases, irregular features in natural terrain, particularly in mountainous regions where most debris flows occur, present challenges for mesh generation or the definition of suitable curvilinear coordinate systems. Moreover, these approaches may require the modeler to anticipate the likely debris-flow path and extent.

Because DEM base data provide elevations at discrete points, a model's numerical discretization (or the generation of derived topographic data sets described above) entails implicit assumptions regarding the smoothness of the underlying surface represented by the raw data. Some modeling approaches rely on continuity or smoothness to achieve numerical accuracy or numerical stability. However, real terrain almost invariably contains irregularities and discontinuities. Such features can include not only natural cliffs but also the vertical faces of some structures such as buildings and dams. In many cases debris-flow interaction with these structures is a prime motivation for performing hazard assessments, and imprecise model representation of their geometries is undesirable.

In our own model, D-Claw, the treatment of DEM data is influenced by the class of numerical methods that we utilize to solve the governing equations (see Sect. 5.8 that follows). It also results in several properties that we consider advantageous for debris-flow modeling. First, the raw DEM data (from one or more possibly overlapping and non-aligned DEM data sets) are used without preprocessing or modification, eliminating the need to interpolate topographic data for debris-flow paths that may be difficult to define in advance. Second, the numerical discretizations (i.e., the computational grids) are not restricted or constrained by the alignment or resolution of the DEM data, although the available DEM resolution(s) may influence accuracy or a modeler's selection of computational grid parameters. Finally, smooth regions as well as topographic discontinuities are represented in the numerical discretization to the degree possible given the raw DEM data. A sharp vertical discontinuity such as a vertical wall at a known location within otherwise coarse DEM data is well-represented by utilizing an intersecting DEM data subset for the structure or feature. Exploiting this representation requires use of numerical methods that are accurate and robust in the presence of such variable DEM resolutions.

In D-Claw we utilize DEM data by employing the following multistep methodology executed during the computation runtime. Initially, the discrete elevation data from a single or multiple DEMs are used to define a piecewise continuous basal surface that intersects the points defined by the most highly prioritized DEM (usually the highest resolution DEM) in any region within the computational domain. The average elevation value of this globally defined surface within a computational grid cell determines a unique elevation value for each cell in the numerical discretization. Therefore, the dynamically derived topographic surface used for the numerical discretization can be interpreted as a piecewise constant surface with step discontinuities at computational cell boundaries. This methodology confers several properties that are advantageous for D-Claw's numerical

solution schemes. First, it preserves volume integrals of the debris lying above the basal surfaces defined by the DEM(s) and derived piecewise constant computational topography for any resolution and alignment of the computational grids, allowing conservation of mass and momentum in the presence of evolving computational grids (see Sect. 5.8 for a description of adaptive mesh refinement). Second, elevation gradients in the DEM data that may represent smooth regions or underlying discontinuities in terrain are retained to the degree possible in the piecewise constant computational grids. Finally, step discontinuities arising from vertical surfaces that are well-defined by intersecting DEMs can be retained in the computational topography.

---

## 5.8 Numerical Solution Techniques

The mathematical core of physically based, depth-averaged debris-flow models is a system of nonlinear hyperbolic partial differential equations (PDEs). This class of PDEs, which arise in diverse problems involving wave propagation, presents unique challenges for obtaining accurate numerical solutions, in part because the equations can have non-unique, discontinuous solutions. The discontinuous solutions apply to (but are not limited to) shock waves, a term borrowed from gas dynamics but also used to describe analogous features such as hydraulic jumps in debris flows (as illustrated in Fig. 5.4 and in Sect. 5.9 below). Standard numerical methods such as classical finite-difference methods are poorly suited for these problems because they may produce physically spurious solutions, numerical dispersion, or numerical instabilities. These shortcomings have motivated the development of specialized classes of numerical solution techniques, including the shock-capturing, finite-volume methods provided by the Clawpack open-source software project (LeVeque, 2002, [www.clawpack.org](http://www.clawpack.org)).

The numerical methods implemented in Clawpack utilize fixed (Eulerian) coordinate systems and analytical wave-propagation

solutions to Riemann problems, a term that describes mathematical problems involving discontinuous steps in values of variables at computational grid-cell interfaces. Originally developed for solving shock-wave problems (Godunov, 1959), the Riemann wave-propagation methodology also provides a logical means for the accurate representation of discontinuous steps in elevation data that may exist when modeling flows across topography represented by DEMs (George, 2008, 2010). The representation of discontinuous steps is particularly relevant for resolving debris-flow fronts moving across steep terrain or impacting vertical structures (See Sect. 5.10 below).

Our D-Claw model uses numerical solution techniques built within the Clawpack framework and on top of the GeoClaw subpackage developed to simulate depth-averaged flows across variable topography (George & LeVeque, 2006; Berger et al., 2011; LeVeque et al., 2011). D-Claw also provides additional numerical strategies aimed at properly resolving balanced steady states (Bouchut, 2004; LeVeque, 2002). Because debris accelerations are absent in such states, the governing conservation equations reduce to steady force balances, which are simple in principle but difficult to satisfy in practice because minuscule numerical imprecision can upset a balanced state, particularly if thousands of numerical iterations are involved. Such balanced steady states exist, for example, in static bodies of water overlying variable bathymetry (George, 2008) and in static masses of sediment resisting downslope gravitational forces prior to the onset of debris-flow motion (George & Iverson, 2014; George et al., 2022; Iverson & George, 2016). Thus, maintaining well-balanced steady states plays a particularly important role when statically balanced initial debris conditions are considered (see Sect. 5.6 above).

Additional numerical challenges exist because many hyperbolic problems, including those that arise in depth-averaged modeling of debris flows, feature a broad spectrum of spatial scales that vary in time, location, and extent. This breadth of scales motivated the development of a computational strategy known as

adaptive mesh refinement (AMR) (Berger and Olinger 1984), which utilizes evolving patches of nested computational grids with varying cell sizes based on dynamic features of the numerical solution. Various implementations of AMR exist, but the aim of all AMR techniques is to provide optimal grid resolutions for attaining numerical accuracy and computational efficiency throughout the duration of a simulation.

Standard AMR techniques developed for general hyperbolic conservation equations are not well-suited for modeling depth-averaged shallow flows moving across variable topography, because the techniques cannot simultaneously preserve balanced steady states (such as static states) and conserve mass, momentum, and energy. Specialized AMR techniques were developed to overcome this problem in the context of tsunami modeling (George & LeVeque, 2006; LeVeque et al., 2011). The techniques were later extended to modeling of general depth-averaged flows over topography such as overland floods (Berger et al., 2011; George, 2010) and debris flows (George & Iverson, 2014).

Use of the specialized AMR algorithms that preserve balanced states also enables D-Claw to use evolving, high-resolution grids to dynamically resolve advancing flow fronts moving through complex terrain, while retaining coarse grids where no evolution of variables occurs (e.g., as in those parts of the computational domain where flow is absent). This approach makes possible the use of modern sub-meter-resolution DEM data only where it is needed within a large domain. By doing so, use of AMR in D-Claw dramatically affects the simulation results where there are important yet small-scale topographic features at isolated locations (for example, dams, levees, buildings, and so on), which require fine grid resolutions that would be prohibitive computationally if applied to the entire domain.

An alternative open-source software package, *r.avaflow* (Mergili et al., 2017), solves the two-phase depth-averaged debris-flow equations of Pudasaini (2012). Like D-Claw, *r.avaflow* employs Eulerian numerical methods developed

specifically for hyperbolic systems of differential equations. However, it utilizes total variation diminishing non-oscillatory central differencing (TVD-NOC) numerical solution schemes (Nessyahu & Tadmor, 1990), which have been successfully applied to mass flow problems more generally (see Mergili et al., 2017, for examples). Unlike D-Claw, ravaflow solves equations in local terrain-fitted coordinates. This approach confers some advantages in terms of physical fidelity, but it can present practical challenges for modeling flows across complex, real-world topography. For instance, variables expressed in local terrain-fitted coordinates and DEMs expressed in spatially uniform Cartesian coordinate systems are not always compatible. In general, a transformation of variables computed in terrain-fitted coordinates to uniform Cartesian DEM coordinates is necessary, and it must be approximated (Mergili et al., 2017).

Another approach for tackling the difficulty of accurately modeling shallow flows across rugged topography is implemented in the model SHALTOP (Bouchut et al., 2003; Lucas et al., 2007), which solves model equations in global Cartesian coordinates but corrects the equations in order to satisfy the shallowness assumption applied in the local bed-normal direction. This approach can capture bed-normal accelerations due to terrain curvature (Peruzzetto et al., 2021), but it still requires that bed-normal variables be transformed to a Cartesian reference frame as represented by a standard DEM. Like D-Claw, SHALTOP utilizes well-balanced finite-volume numerical schemes for solving hyperbolic systems of differential equations (Bouchut, 2004).

Other Eulerian debris-flow models include TITAN2D (Pitman et al., 2003), which solves single-phase depth-averaged equations, and RAMMS (Christen et al., 2010), which was originally developed for modeling snow avalanches but utilizes a single-phase Voellmy flow resistance formula for modeling debris flows. These models employ finite-volume solution schemes broadly similar to those used in D-Claw.

A more distinctive method for solving the hyperbolic system of PDEs in depth-averaged

debris-flow models is the meshless Lagrangian method known as smooth-particle hydrodynamics (SPH) (McDougall & Hungr, 2004). As opposed to Eulerian methods, Lagrangian methods formulate the model PDEs in a moving frame of reference that translates with the flow. In applications of SPH to debris flows, the continuum mechanical representation of debris-flow material is effectively replaced by a collection of interacting, columnar “particles” that span the flow thickness as they move downstream (McDougall & Hungr, 2004). Moreover, SPH removes the effects of discontinuities in solutions of the governing PDEs by using a smoothing formula to average particle-interaction mechanics among groups of neighboring particles.

In some respects the SPH methodology codifies a modeling philosophy that is the opposite of that of D-Claw. Whereas SPH produces smoothed results, the shock-capturing AMR methodology of D-Claw aims to preserve the effects of discontinuities and the details of abrupt flow-dynamics features such as hydraulic jumps and flow interactions with vertical barriers. Each of these methodologies—as well as other numerical methodologies—may have advantages in different circumstances. However, we are unaware of any application of SPH methodology to two-phase debris flows in which the debris solid volume fraction, bulk density and apparent rheology naturally coevolve as flow dynamics evolve.

---

## 5.9 Computer Source Code Verification and Accessibility

A problematic aspect of computational modeling of complex natural phenomena such as debris flows is that appealing graphical results may be generated even if the underlying model is inadequate from a scientific perspective. (Few scientists would deny that Hollywood movie animators are adept at generated numerical output that superficially resembles disastrous natural phenomena, ranging from tornadoes to tsunamis to asteroid impacts, but few animators

would claim that their model outputs have scientific validity merely because they look good.) The value of scientific numerical models cannot be judged solely on the basis of the appearance of their output. Instead, the models should be thoroughly documented, tested, and available for scrutiny, and a key component of such models is the computer source code.

Just as thorough derivations of debris-flow model equations should be freely available for critical inspection and validation by prospective model users, computer source codes that are used to solve the equations and generate output should also be freely available. No scientific computation should involve use of proprietary computer source code that is inaccessible for independent verification. Source code errors or inadequacies are commonly revealed only through scrutiny of the code by diverse users who pursue diverse applications, and issues may never be revealed if the source code remains in a black box.

Trujillo-Vela et al. (2022) provide an extensive table summarizing source code accessibility as well as some other properties of many debris-flow models, landslide models, and granular-avalanche models. The table contains some errors, but it is nevertheless useful. We have avoided presenting a similar table here, in part because it would largely reproduce that of Trujillo-Vela et al. (2022), and in part because it is difficult to ensure that the content of such tables is accurate. Many models are presented and utilized without full disclosure of all of their salient details, making it challenging for others to evaluate the models thoroughly or characterize them accurately.

In the twentieth century scientific computer source codes were commonly printed out in full and made available for inspection, but full printouts of recently developed source codes typically aren't available. Modern computer source codes can be long and complex, and they can evolve with time as improvements and additions are made. Consequently, developers of some scientific codes have adopted practices established in computer science and software engineering.

These practices include the use of version control systems (e.g., subversion, git), open-source licensing, and freely available source-code repositories. Our model D-Claw has been developed following these practices, and its components are publicly hosted on github.com (see Mandli et al., 2016, [www.github.com/clawpack](http://www.github.com/clawpack), and [www.github.com/geoflows/D-Claw](http://www.github.com/geoflows/D-Claw)).

LeVeque (2013) suggested that all aspects of computational procedures used to generate scientific output, including post-processing programs used to generate graphical representations of output, ought to be fully documented and freely accessible for scrutiny. Similar views have been expressed by others in the computational sciences (e.g., Barnes, 2010; Peng, 2011; Stodden et al., 2016). It is difficult to argue against this full-disclosure protocol if reproducibility and verifiability of model output is the objective.

---

## 5.10 Model Testing

Systematic testing of the predictions of debris-flow models should precede use of the models for hazard assessment, but conclusive model testing can be hampered by the effects of uncertainties about initial flow volumes, auxiliary conditions, or appropriate values of parameters or tuning coefficients. Nonetheless, experimental data and well-documented historical debris flows afford opportunities for model testing that is more rigorous than is generally possible for models of geological processes that occur in deep Earth or deep time.

Depth-averaged debris-flow models can potentially predict a wide range of quantities, each of which can be used for model testing. The most rigorous tests involve testing of model predictions against several quantities measured simultaneously. All depth-averaged models of debris-flow motion across three-dimensional terrain predict values of flow depth  $h(x, y, t)$  and two flow velocity components,  $u(x, y, t)$  and  $v(x, y, t)$  (which yield two flow momentum components,  $\rho uh(x, y, t)$  and  $\rho vh(x, y, t)$ ), as described in Sect. 5.3 above. Therefore, direct

tests of model predictions can be made when direct measurements of these evolving quantities at various locations are available, and these tests can be expanded if there are simultaneous measurements of additional quantities such as basal shear stresses, total normal stresses and pore-fluid pressures. Reproducible measurements of these co-evolving quantities generally can be made only in idealized experimental settings (cf. George & Iverson, 2014; Iverson et al., 2010), but some analogous measurements have been made in carefully instrumented cross sections constructed at field sites (McArdell et al., 2007; McCoy et al., 2010). The spatial distributions and thicknesses of natural debris-flow deposits also afford opportunities for model tests, although predictions of these quantities are strongly influenced by assumptions about initial conditions—especially concerning initial flow volumes, velocities, and depths (Barnhart et al., 2021b). In some circumstances the seismic signatures of large natural debris flows can be used for testing model predictions of temporally varying momentum exchanges between debris flows and their beds (Moretti et al., 2015). Runup heights measured where natural debris flows encounter obstacles in their paths can be used in a similar manner, particularly if independent constraints on flow velocities exist (e.g., Allstadt, 2013).

Here we illustrate some tests of our own debris-flow model, D-Claw, against the results of large-scale laboratory experiments and a  $\sim 50 \times 10^6 \text{ m}^3$  debris flow that occurred in 2010 at Mount Meager, British Columbia, Canada. Each type of test serves a particular purpose for evaluating model simulations of debris-flow onset, flow dynamics, or extent of downstream inundation. No single test is definitive, but confidence in any model grows if it performs well in a variety of tests.

### 5.10.1 Debris-Flow Mobilization from Landslides

Mobilization of debris flows from landslides provides a model-testing benchmark problem because it involves a precisely defined initial condition (static mechanical equilibrium of a wet sediment mass) and because the physical properties of static debris are readily measured. Many experiments on debris-flow mobilization from landslides have been performed at the U.S. Geological Survey (USGS) debris-flow flume (Iverson et al., 1997, 2000; Logan et al., 2007; Reid et al., 1997). Figures 5.7 and 5.8 illustrate the results of D-Claw simulations of one of these experiments, conducted on 17 June 1998. The experiment was described in detail by Iverson et al. (2000) and documented in video recordings that are viewable online (Logan et al., 2007). In the experiment a liquefying landslide was triggered by slowly adding groundwater to a  $6 \text{ m}^3$  static prism of loosely packed, moist debris resting on the  $31^\circ$  concrete flume bed and held in place by a rigid retaining wall. When basal pore pressures became large enough, the slope began to fail (at  $t=0$  in Fig. 5.7). Then, over the course of about 1 s, the failing debris liquefied in response to porosity contraction and attendant pore-pressure increase. The liquefied debris flowed over the retaining wall and then down a ramp and onto the flume bed, as illustrated in the last few frames of Fig. 5.7 (George & Iverson, 2014).

The accuracy of the modeled behavior depicted in Fig. 5.7 can be tested quantitatively by comparing it with sensor data collected during the experiment. Data from two ground-surface extensometers and three pore-pressure sensors buried at different depths are shown in Fig. 5.8 along with two sets of model predictions for a 2 s period that spans the time of slope

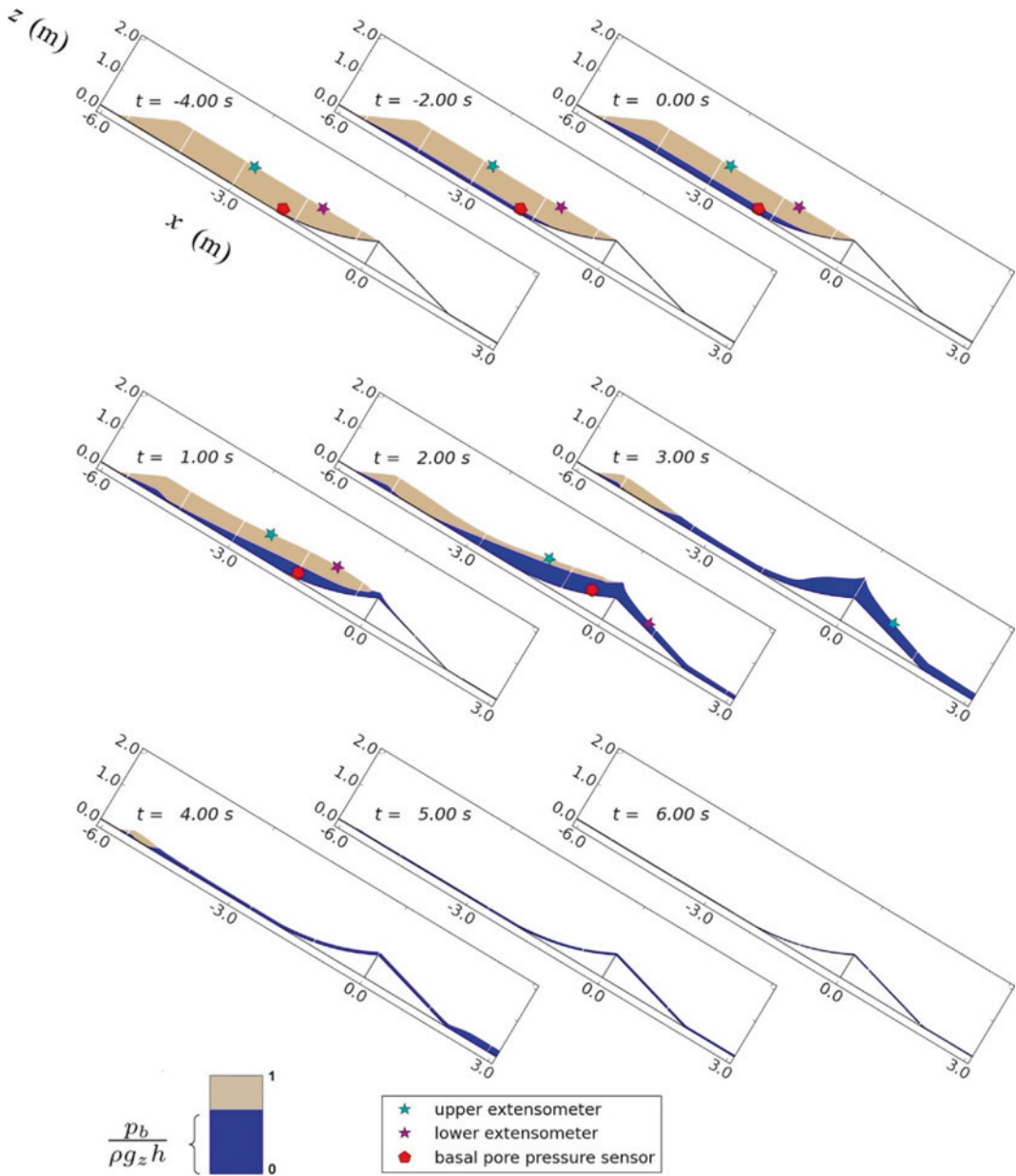


**Fig. 5.7** Time sequence of vertical cross-sectional views of a D-Claw simulation of a liquefying landslide at the USGS debris-flow flume on 17 June 1998 (after George & Iverson, 2014). The relative height of blue shading within the brown-shaded landslide mass depicts the basal pore-water pressure  $p_b$  as a fraction of the total lithostatic basal normal stress,  $\rho_g z h$ . A condition of complete liquefaction is indicated by  $p_b/\rho_g z h = 1$  and full blue shading. Symbols show the positions of surface extensometers and the basal pore-pressure sensor

used to test model predictions, as illustrated in Fig. 5.8. The sensors are motionless until  $t=0$ , when slope failure commences. They subsequently move with the sediment and pass over the retaining wall and ramp centered at  $x=0$  m. The shape of the curved basal surface of the sediment mass just upslope from the bed-normal retaining wall is defined by data from a stack of tiltmeters that revealed the location of the basal slip surface (Iverson et al., 2000)

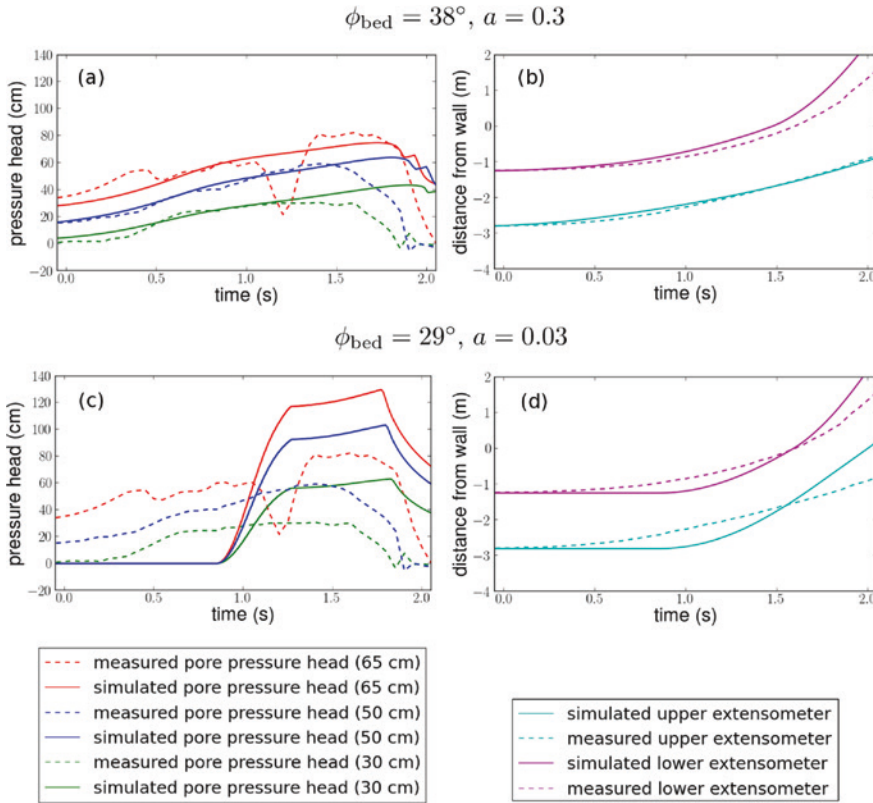


**Fig. 5.8** D-Claw model output (solid lines) compared with extensometer data and piezometer data measured at initial depths of 65, 50 and 30 cm (dashed lines) in the flume debris-flow mobilization experiment conducted on 17 June 1998 (after George & Iverson, 2014). Time  $t=0$  indicates the onset of detectable landslide motion.

Sensors translated with the moving landslide mass as illustrated in Fig. 5.7. D-Claw output using a  $38^\circ$  basal friction angle is shown in panels a and b, and output using a  $29^\circ$  basal friction angle is shown in panels c and d. The dimensionless parameter  $a$  is proportional to the debris compressibility (Iverson & George, 2014)

failure and liquefaction. The two sets of model predictions differ in one important respect: one set uses an independently measured value of the friction angle of debris in contact with the concrete flume bed ( $29^\circ$ ) and the other set uses a friction angle increased to  $38^\circ$  to improve the fit to the experimental data (Fig. 5.8). The increased friction angle helps account for the influence of flume sidewall friction that was not explicitly represented in the depth-averaged numerical simulations (George & Iverson, 2014). The two sets of predictions also use differing values of a dimensionless coefficient  $a$ , which is proportional to the debris compressibility and is not as well-constrained as other debris properties (Iverson & George, 2014).

Figure 5.8 shows that a modest improvement of model predictions results from use of adjusted values of the basal friction angle and the coefficient  $a$ , but more importantly, it shows that each set of model predictions provides a reasonably good picture of the coevolution of several dependent variables as slope failure occurred and debris liquefaction ensued. Consequently, we infer that the underlying physics represented by the model is approximately correct. If the values of fewer dependent variables were predicted simultaneously, then model tests would be weaker and inferences about model validity would be more equivocal. It is desirable whenever possible to test debris-flow models against such multivariate data.

### 5.10.2 Debris-Flow Runup

Runup of debris flows on barriers or adverse slopes can provide model-testing opportunities because runup occurs commonly and maximum runup heights can be measured with confidence. However, in most field settings, debris-flow dynamics prior to the onset of runup are poorly constrained. In this section we compare D-Claw simulations of runup with observations obtained in experiments conducted with  $10 \text{ m}^3$  debris flows at the USGS debris-flow flume. An advantage of the experiments is that flow speeds and depths prior to runup were precisely measured, eliminating a source of uncertainty in model testing (Iverson et al., 2016).

Runup that occurs when a debris flow encounters a vertical barrier is most significant when the incoming flow is supercritical and an abrupt conversion of kinetic energy to potential energy generates a shock (i.e., hydraulic jump). Runup of subcritical debris flows is less significant because subcritical flows merely decelerate and accumulate as “backwater” deposits when they encounter a barrier. Figure 5.9 compares snapshots of D-Claw simulations with time-stamped video frames that depict a supercritical  $10 \text{ m}^3$  debris flow running up approximately 2 m on a rigid vertical wall. Details of the debris properties and parameter values used in the simulations were presented by Iverson et al. (2016). The flow generating the runup had multiple surges, the largest of which is visible in Fig. 5.9 exiting the flume mouth at  $t=10.12 \text{ s}$ . Both constructive and destructive interference of successive debris-flow surges strongly influenced runup behavior in this experiment and in the model simulations by transiently increasing or decreasing the runup height (Iverson et al., 2016). Analogous interactions of surges can be difficult to decipher from runup deposits in the field.

Runup can also occur when debris flows encounter adverse slopes and travel some distance up their faces. Model tests against data from debris-flow flume experiments addressed this scenario by using a 30-degree adverse slope

with a width of 3 m, so that some debris spilled off the edges of the slope as runup occurred when a  $10 \text{ m}^3$  debris flow discharged from the mouth of the 2-m wide USGS debris-flow flume (Fig. 5.10). Details of the slope configuration and bed roughness were described by Iverson et al. (2016).

As in the vertical barrier case, runup on the adverse slope was influenced by arrival of successive surges of flow and by the development of a shock. However, shock development on the 30-degree slope was preceded by a smooth upslope flux of momentum, as illustrated in the upper frames of Fig. 5.10. The D-Claw model accurately simulated the transition from this smooth momentum flux to a shock-interrupted flux. It also accurately simulated the maximum runup height, which developed as the peak shock collapsed and shunted some debris both upslope and downslope (final frames in Fig. 5.10).

Successful testing of the D-Claw model (or any other debris-flow model) under the controlled, reproducible conditions described above can bolster confidence in the model. It can also prompt a next step in testing: application to historical real-world debris flows that are more complicated than experimental debris flows but are reasonably well-constrained by observations and data.

### 5.10.3 Mount Meager Debris-Flow Dynamics

One of the world’s largest debris flows in recent decades began as a landslide on the south flank of Mount Meager volcano in British Columbia, Canada on 6 August 2010. Most of the  $\sim 50 \times 10^6 \text{ m}^3$  landslide mobilized as a debris flow that descended the steep, tortuous valley of Capricorn Creek before it reached a confluence with Meager Creek and ran up to height of 270 m on an adjacent mountainside (Fig. 5.11). Much of the debris then traveled downstream along the Meager Creek drainage and onto the broad floodplain of the Lillooet River, but some

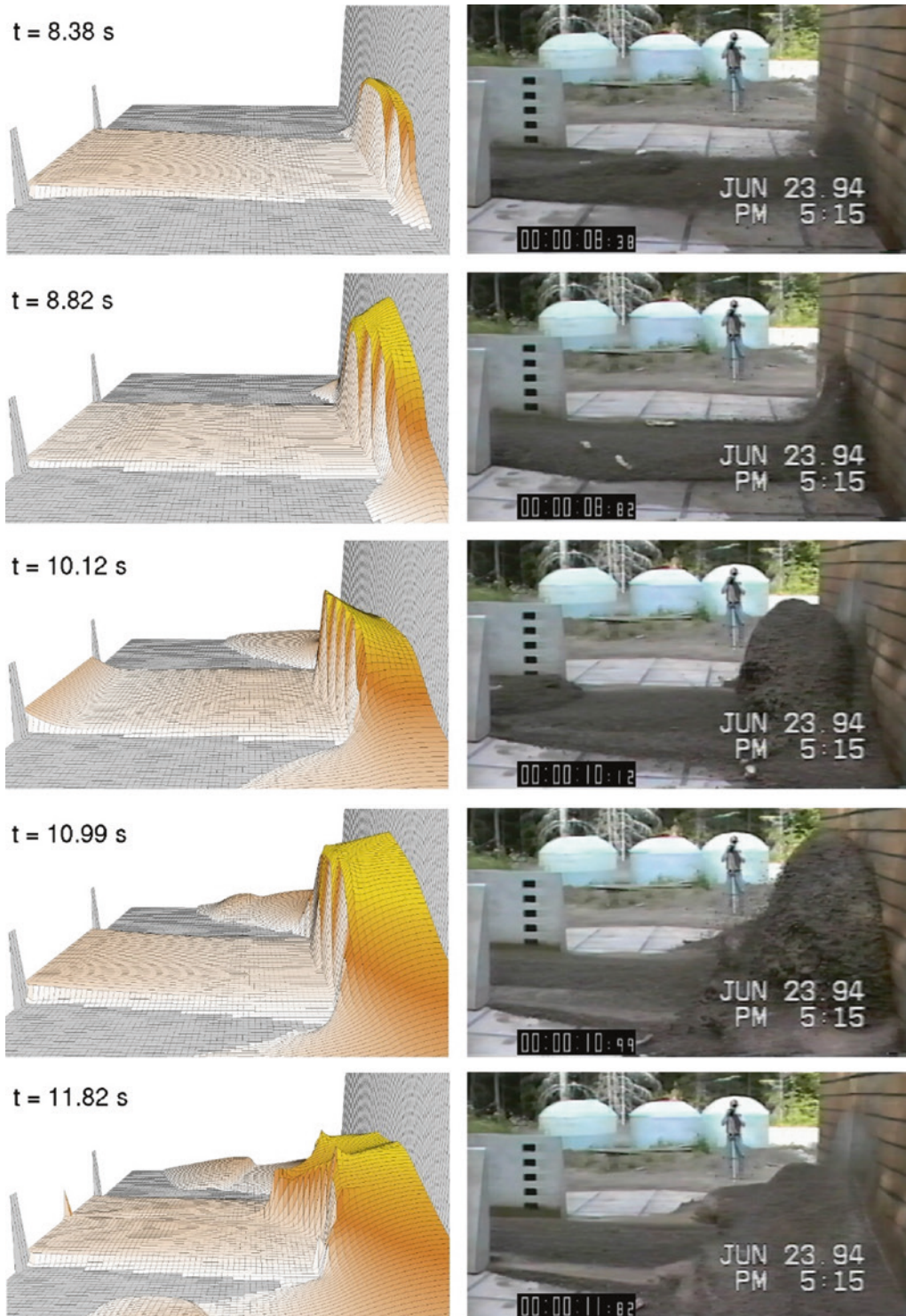


**Fig. 5.9** Time sequence of oblique 3-D perspective views of a D-Claw simulation (left column) and corresponding video frame captures (right column) of a vertical barrier runup experiment at the USGS debris-flow flume on 23 June 1994. Measured incoming flow properties

were used to initiate the numerical simulation. Timestamp in each frame of model results and video recordings refers to the time since the flume headgate began to open. An animated version of this figure is available as Movie S5 in the Supporting Information of Iverson et al. (2016)

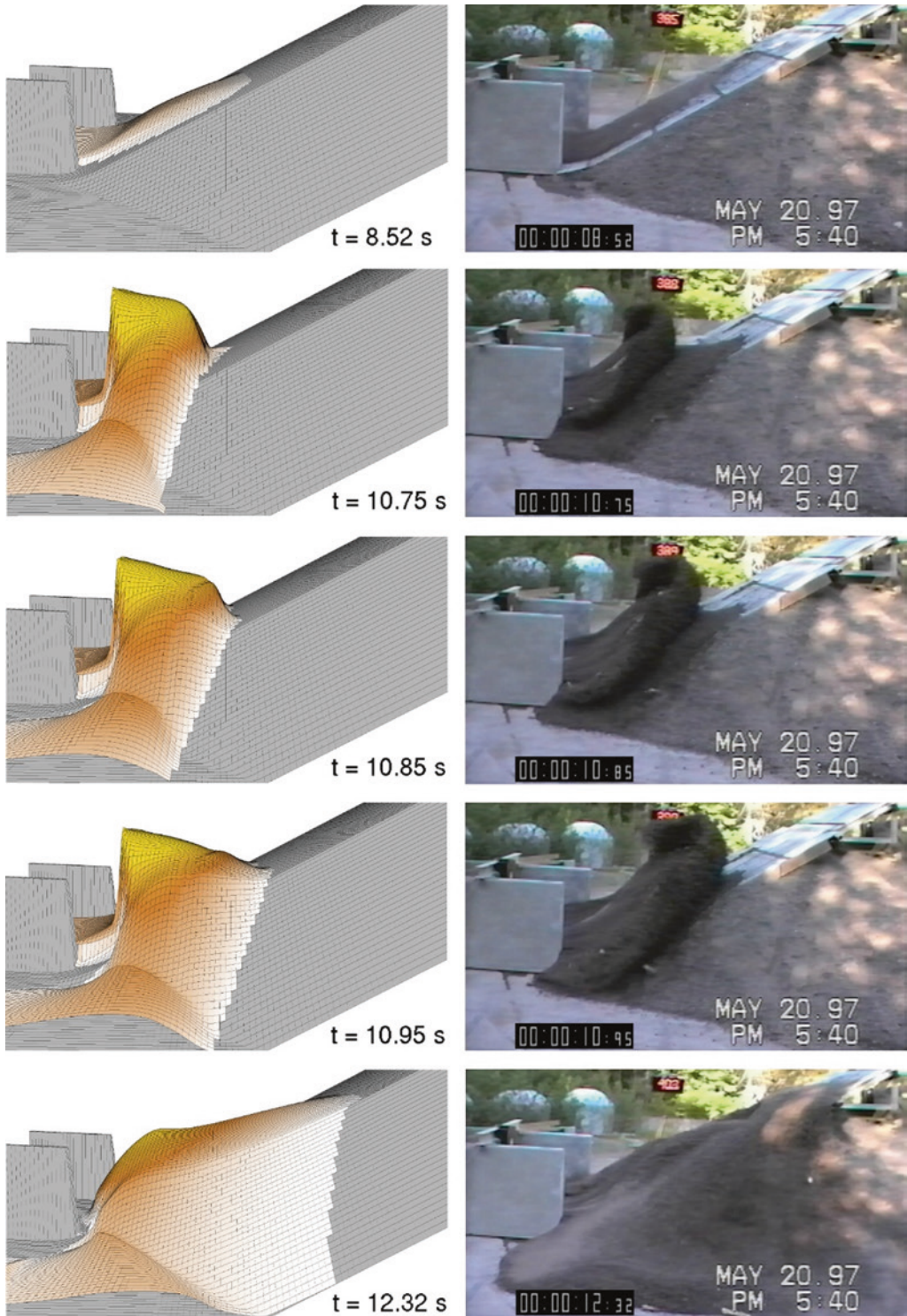


**Fig. 5.10** Time sequence of oblique 3-D perspective views of a D-Claw simulation (left column) and corresponding video frame captures (right column) of an adverse-slope runup experiment at the USGS debris-flow flume on 20 May 1997. Measured incoming flow

properties were used to initiate the simulation. Timestamp in each frame of model results and video recordings refers to the time since the flume headgate began to open. An animated version of this figure is available as Movie S6 in the Supporting Information of Iverson et al. (2016)



**Fig. 5.11** Oblique aerial photographs of the site where the 2010 Mount Meager debris flow ran up 270 m vertically on the mountainside at the confluence of Capricorn and Meager Creeks, located at 50.606°N/123.430°W.

Red arrow in the small inset photo shows the approximate look angle of the camera used to take the large photo. Photos courtesy of Dave Steers

debris traveled more than 3 km upstream along the Meager Creek valley.

The 2010 Mount Meager landslide/debris flow was thoroughly examined in several studies, beginning with that of Guthrie et al. (2012). Some of the studies inferred the detailed chronology of the event through analysis of the long-period seismic energy radiated by the moving mass (e.g., Allstadt, 2013), and some involved modeling the event numerically (e.g., McDougall, 2017; Moretti et al., 2015). Knowledge gained from these studies and detailed field work by Roberti et al. (2017, 2018) makes the Mount Meager landslide/debris flow better understood than most events of comparable scale.

Here we describe a D-Claw simulation of the Mount Meager landslide/debris flow as it interacted with complex topography. The event provides a multifaceted test of model capabilities because it involved a combination of

gravitational failure of a static mass, flow down a tortuous path that bifurcated at the confluence of Capricorn and Meager Creeks (with some debris traveling upstream), flow runup, and flow spreading and deposition on the broad Lillooet River floodplain. The resolution of our numerical simulation is limited by the coarse horizontal resolution (20 m) of the pre-event DEM available for the Mount Meager area, but in D-Claw's application of AMR we bolster computational accuracy by specifying a maximum computational grid resolution of 10 m. With this resolution, D-Claw simulations of the entire slope failure/landslide/debris-flow sequence are completed in less than an hour on a desktop computer.

The values of most parameters used in our D-Claw simulation of the Mount Meager event are the same as values discussed in detail by Iverson and George (2016) for our best-fit simulation of a large, liquefying landslide that

occurred near Oso, Washington, USA in 2014. However, significant differences exist in the values of the sediment basal friction angle ( $42^\circ$  for Mount Meager versus  $36^\circ$  for Oso) and the initial sediment hydraulic permeability ( $5 \times 10^{-10} \text{ m}^2$  for Mount Meager versus  $1 \times 10^{-8} \text{ m}^2$  for Oso). The larger basal friction angle for Mount Meager is required to balance forces within the initially static rock/sediment mass, which occupied a slope much steeper than that at Oso. The smaller hydraulic permeability for Mount Meager reflects the presence of fine-grained sediment derived from hydrothermally altered volcanic rock, which causes the modeled Mount Meager debris to remain liquefied longer than the debris at Oso. Thus, for our Mount Meager simulation neither the friction angle nor permeability values were measured directly, but their assigned values are consistent with physical evidence.

As in the Oso case, onset of slope failure in our Mount Meager simulation is triggered by imposing gradually rising basal pore pressures that perturb the balanced static state. The geometry of the failing mass at Mount Meager is specified by using a method detailed in prior publications on the Oso event (Iverson & George, 2016; Iverson et al., 2015). In brief, the method involves creation of a smooth basal failure surface beneath the pre-event topography so as to replicate the observed  $\sim 50 \times 10^6 \text{ m}^3$  landslide volume and match the observed perimeter of the landslide source area.

We stress that the simulation of the Mount Meager event we present here is not comprehensive because it does not consider diverse possible scenarios for the onset of motion and does not consider many of the geological complexities that were recognized after the event occurred (cf. Guthrie et al., 2012; Moretti et al., 2015; Roberti et al., 2017, 2018). Precise accounting for *ex post facto* observations is not our intention. Instead, our goal is testing of a model designed to be useful for prediction, and predictions never benefit from the clarity offered by post-event hindsight. Thus, rather than trying to mimic the precise geological character of the Mount Meager debris-flow source area

materials, geometry, and failure sequence, we use an approach that might be described as “intentionally naïve” in order to test how our model performs when using a limited amount of a priori information.

A map view of the overall behavior of our Mount Meager simulation (Fig. 5.12) illustrates the debris flow’s rapid initial acceleration and descent of Capricorn Creek, where the flow reached inferred speeds as high as  $\sim 90 \text{ m/s}$  (Allstadt, 2013; Guthrie et al., 2012). Approximately 140 s after the onset of slope failure, the modeled flow front reaches the T-shaped confluence of Capricorn Creek with Meager Creek, and runup on the adjacent mountainside quickly ensues (Fig. 5.13). This timing is consistent with the timing inferred from seismological evidence (Allstadt, 2013). Simulated runup behavior includes development of a shock (i.e., hydraulic jump), and it resembles the runup behavior observed in flume experiments with debris flows encountering an adverse slope (Fig. 5.10).

During and following runup, the simulated debris flow bifurcates and travels upstream as well as downstream in the valley of Meager Creek (Figs. 5.12 and 5.13). The runup process influences this bifurcation because a reversal of flow momentum occurs as the debris running up the mountainside collapses back into the Meager Creek valley, where it collides with debris still arriving from upstream via Capricorn Creek. The details of such a collapse-and-collide process cannot be inferred with confidence from field observations of deposits, but the simulation is consistent with field evidence of the maximum 270 m runup height, and it provides insight to the possible sequence of events during the flow bifurcation.

Following debris-flow bifurcation, the simulated inundation of the Lillooet River floodplain occurs relatively slowly as the advancing debris flow loses speed and eventually stops (Fig. 5.12). This part of the simulation appears adequate, but it inspires the lowest degree of confidence because nuances of topographic steering and frictional energy dissipation play an increasingly prominent role as the modeled

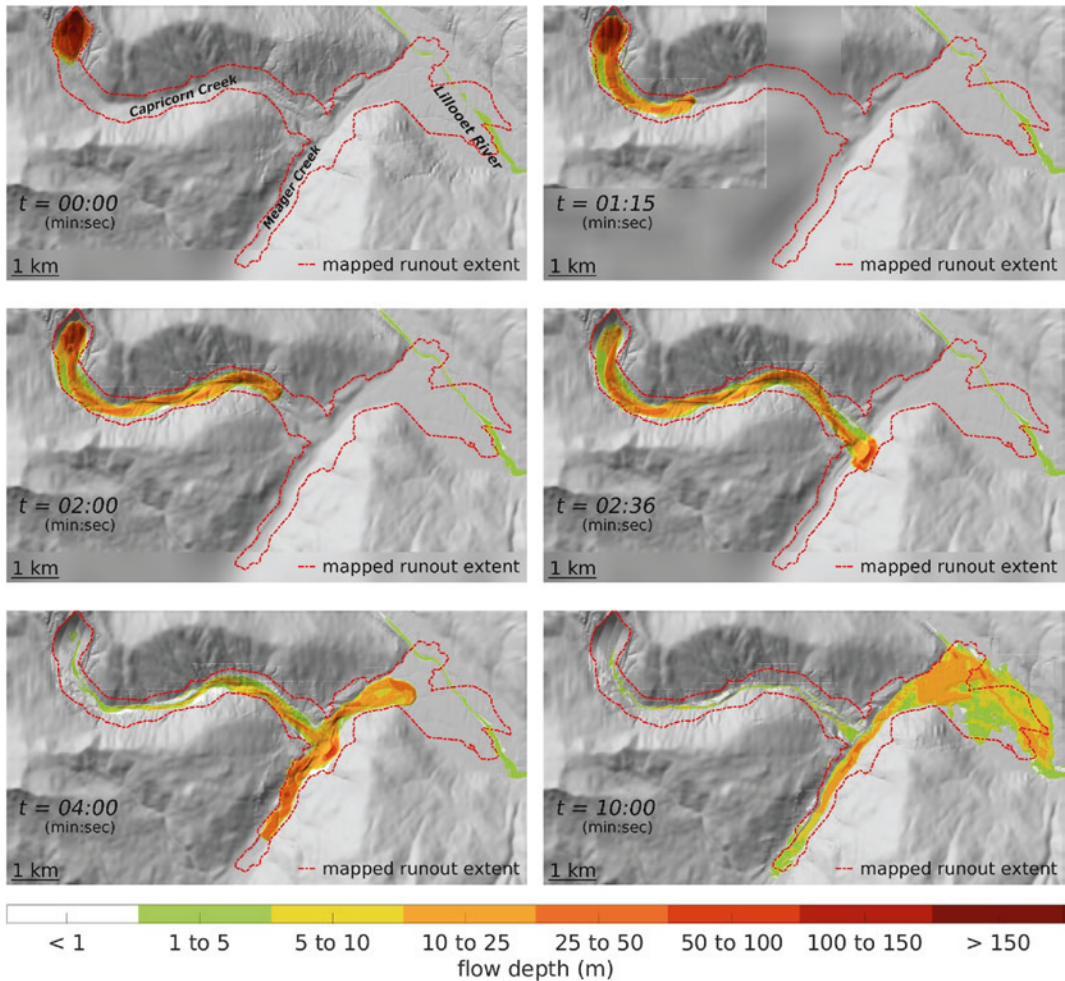


**Fig. 5.12** Time sequence of shaded-relief maps of a D-Claw simulation of the 2010 Mount Meager landslide/debris flow, illustrating the distribution of debris thicknesses at selected times ( $t$ ) after the onset of motion. The first frame ( $t=0$ ) shows the initial, static landslide mass, and the final frame ( $t=10$  min) shows the distribution

of static deposits at the conclusion of the simulation. The dashed red line shows mapped flow path boundaries inferred from satellite imagery. Shaded relief appears blurry where D-Claw's use of AMR affords very low resolution

debris-flow slows and momentum fluxes play a diminishing role. Whereas conservation of momentum and formulation of numerical methods to ensure that momentum is conserved are very solidly grounded in physical law and mathematical analysis, specification of frictional forces that cause flow stoppage is an inexact science. DEM representation of topographic subtleties that influence the margins of modeled deposits is similarly inexact.

We note that prediction of the extent of debris-flow runout paths has great practical importance but also that matching the observed distribution of downstream debris-flow deposits provides an insufficient test of D-Claw or any other debris-flow model. Better tests are possible if, in addition to observational constraints on runout extent, there are observational constraints on flow dynamics and the distributions of statically balanced material in debris-flow source

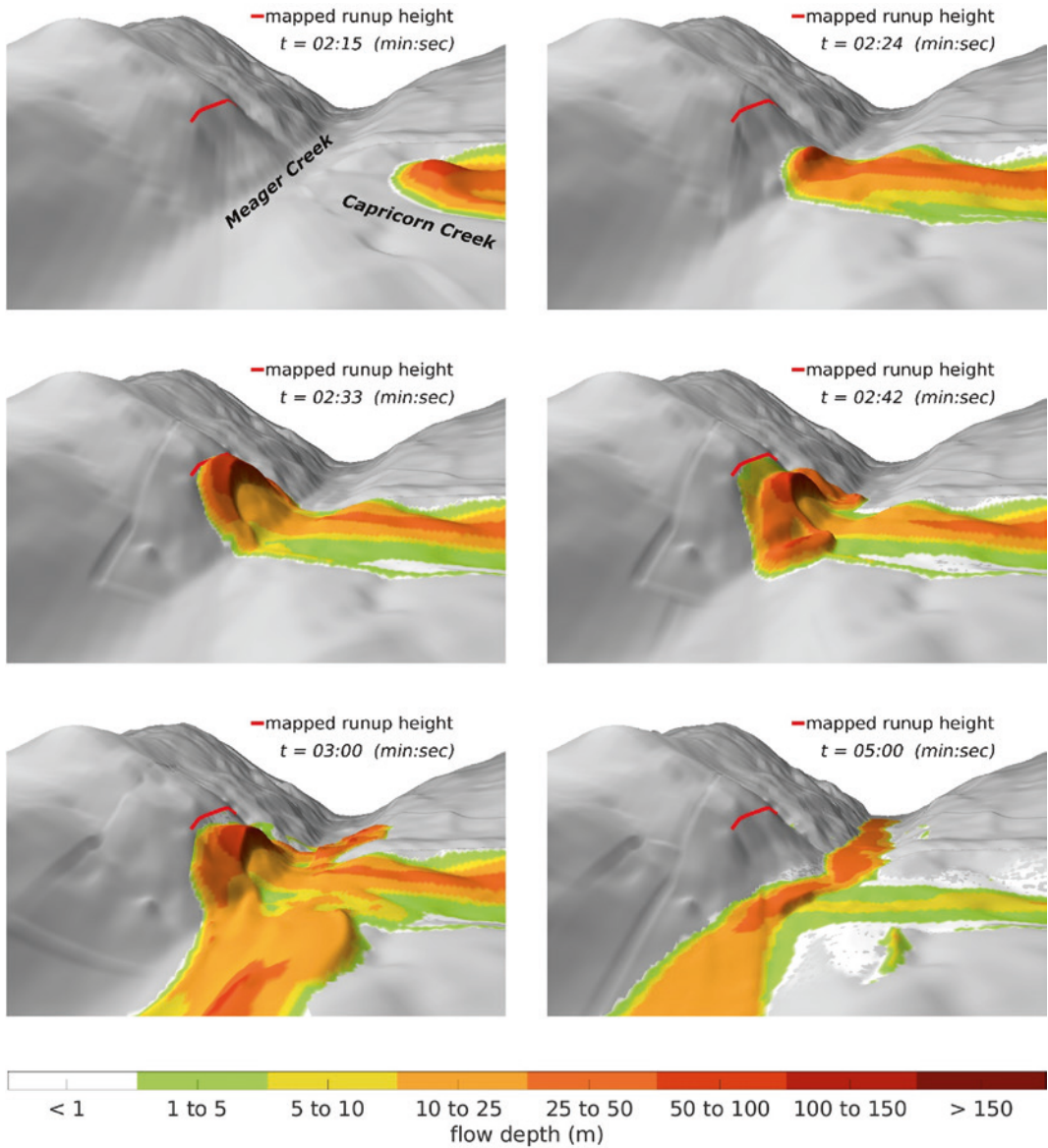


**Fig. 5.13** Time sequence of oblique shaded relief images of a D-Claw simulation of the Mount Meager debris flow running up to a vertical height of 270 m, shown by a red marker line on the mountainside adjacent

to the T confluence of Capricorn and Meager Creeks. Times ( $t$ ) shown in each frame refer to the time elapsed since the onset of landslide motion at  $t=0$

regions. The presence of these constraints makes the Mount Meager case well-suited for testing of numerical models, irrespective of the coarse resolution of the pre-event DEM for the area.

### 5.11 Model Application to Hazard Forecasting

Application of numerical models to debris-flow hazard forecasting poses several challenges that don't arise when modeling debris flows



is named T-260-HM to distinguish it from the other seven scenarios modeled by George et al. (2022).

George et al. (2022) used  $260 \times 10^6 \text{ m}^3$  as the maximum credible volume of an unheralded lahar at Mount Rainier because it matches the estimated volume of the largest documented prehistoric lahar that has occurred there without evidence of accompanying eruptive activity (i.e., the Electron Mudflow, Scott et al., 1995). The study used the Tahoma Glacier headwall as a probable lahar source area because it has been identified as the part of Mount Rainier most prone to slope failure due to its steep slopes and abundance of weak, hydrothermally altered rock (Reid et al., 2001). Within the headwall region, George et al. (2022) constructed a landslide basal slip surface so that the source area conformed with natural topographic boundaries and enclosed the desired  $260 \times 10^6 \text{ m}^3$  of material, including glacial ice (cf. Iverson & George, 2016; Iverson et al., 2015). As in our Mount Meager simulation, motion of material within the source area was instigated by gradually raising basal pore-fluid pressure until slope failure began in the weakest area. Failure then propagated to adjacent areas by momentum exchange.

The Mount Rainier D-Claw simulations of George et al. (2022) distinguished high-mobility lahars from low-mobility events by employing different values of the debris hydraulic permeability,  $k$  (cf. Iverson & George, 2016). Simulations with a low debris permeability ( $k = 10^{-11} \text{ m}^2$ ) were used to mimic the behavior of clay-rich, high-mobility lahars in which liquefaction can persist for hours, whereas simulations with a higher permeability ( $k = 10^{-9} \text{ m}^2$ ) were used to simulate low-mobility events in which liquefaction persists for only several minutes. Such low-mobility events exhibit behavior similar to that of some volcanic debris avalanches. Values of key parameters that were held constant in all simulations include those of the basal friction angle, set at  $38^\circ$ , and of the initial difference between the solid volume fraction and quasi-static critical-state volume fraction, set at  $-0.02$ . A detailed discussion of all

parameter values was provided by George et al. (2022).

The subtlety of glacial drainage divides high on the western flank of Mount Rainier causes the simulated T-260-HM lahar to diverge into multiple drainages before funneling into the canyons of the Puyallup and Nisqually Rivers (Figs. 5.14 and 5.15). This flow divergence illustrates the difficulty of anticipating the paths of future lahars in advance, and it highlights the consequent need for large computational domains. Map views of simulation results show that within 8 min of landslide onset, the fronts of the divergent lahar branches descending the Puyallup and Nisqually River valleys travel more than 15 km from their source (Fig. 5.15). Additional map views and animations provided by George et al. (2022) use a larger domain to show the continuation of the simulated lahar paths beyond the margins of Fig. 5.15.

Map views of modeled lahar propagation can be very useful, but for hazard assessment it is important to provide additional information about simulated lahar behavior. For example, Fig. 5.16 shows D-Claw time-series output of lahar depths, speeds, and discharges computed for a location on the Nisqually River floodplain near the community of Ashford, Washington (denoted by a crosshair symbol and the label “4” in Fig. 5.15). At this location the simulated flow front arrives approximately 20 min after landslide onset, followed quickly by peak flow depths close to 14 m and peak flow speeds close to 10 m/s. These values underscore the practical implications of the modeled lahar dynamics in a way that may not be evident from inundation maps alone.

Approximately 20 km downstream from Ashford, the flow of the modeled T-260-HM lahar in the Nisqually River valley is blocked by Alder Dam, a 100-m high concrete structure that impounds Alder Lake reservoir. The reservoir capacity of roughly  $300 \times 10^6 \text{ m}^3$  is similar to the volume of the simulated landslide and lahar shown in Fig. 5.14. Less than half of the volume of the simulated lahar reaches the head of Alder Lake, but upon entering the lake it mixes with

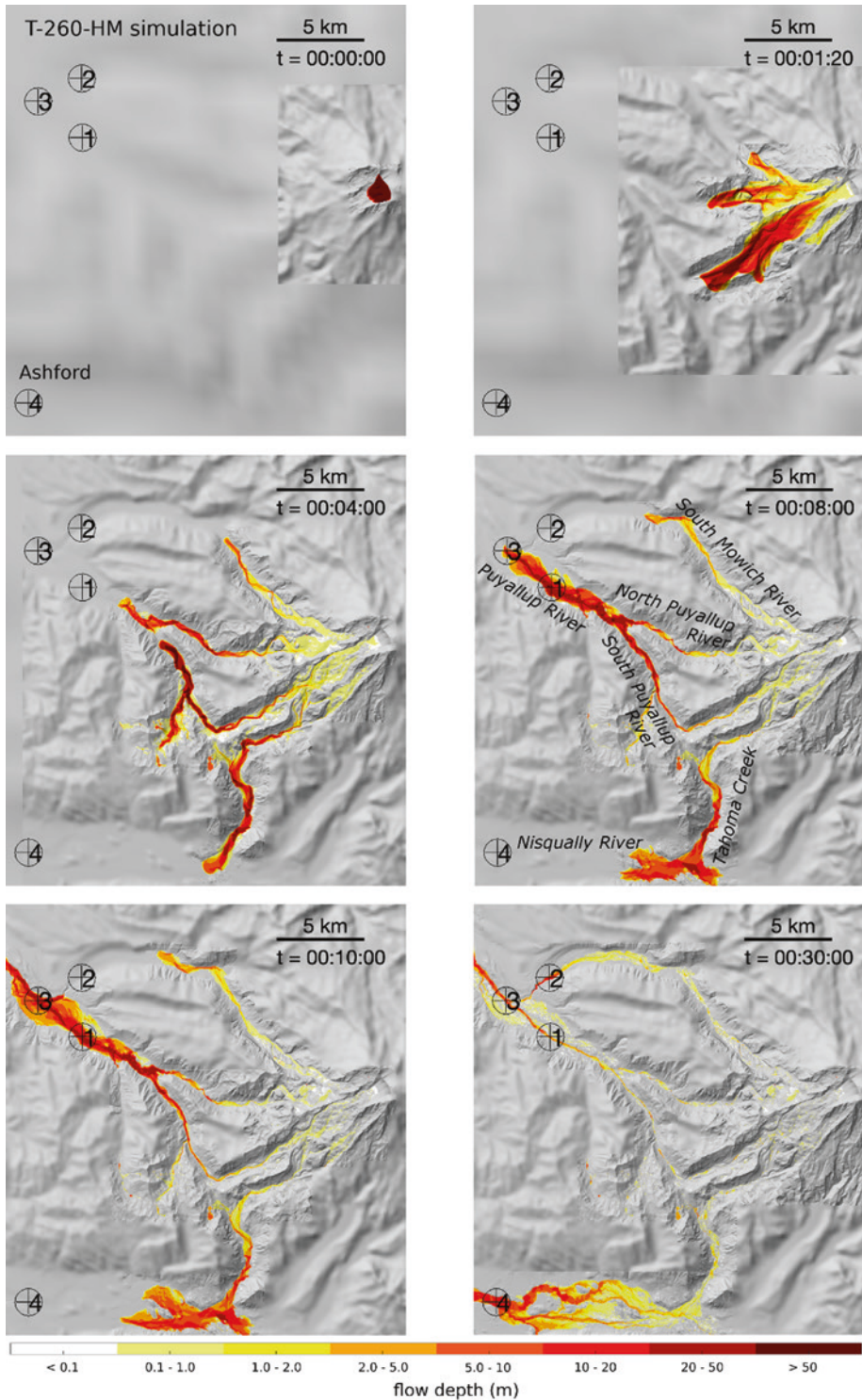


**Fig. 5.15** Time sequence of shaded relief maps showing thicknesses of the simulated T-260-HM lahar at selected times during the first 30 min of motion (from George et al., 2022). Imagery appears blurry where lahar material is absent because D-Claw’s adaptive mesh

refinement employs very coarse resolution in those areas. Circled crosshairs with numbers indicate locations for computation of time-series output similar to that shown in Fig. 5.16. Time (t), in hours:minutes:seconds, refers to the time elapsed since the onset of landslide/lahar motion

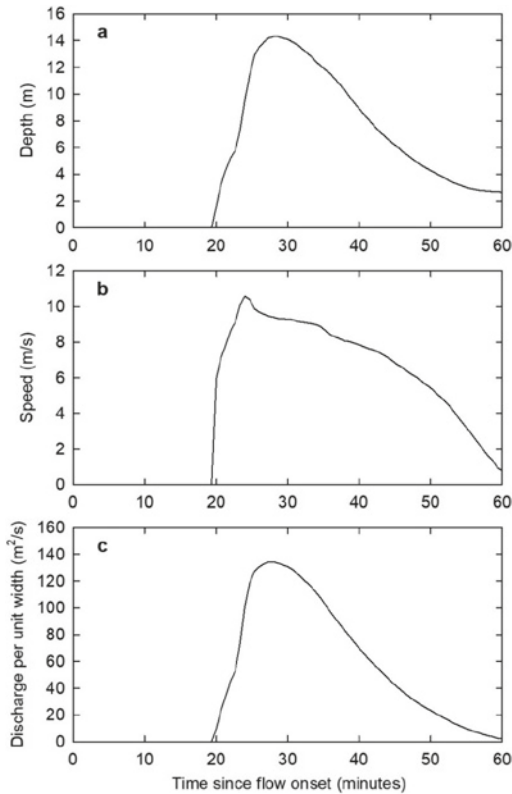


**Fig. 5.16** Graphs of D-Claw time-series output showing the evolution of lahar depths, speeds, and discharges at gauge site 4, located on the Nisqually River floodplain near Ashford, Washington (see Fig. 5.15 for location at the circled crosshair labeled 4). Discharge is given per unit valley width perpendicular to the local flow direction (after George et al., 2022)

and displaces sufficient lake water to cause dam overtopping (George et al., 2022). Figure 5.17 illustrates how D-Claw simulations portray the mixing and overtopping processes for a condition in which the lake's initial water level is 4 m below the dam crest elevation. An important finding of the simulations is that the effects of dynamic wave propagation caused by lahar entry into the shallow headwaters of the reservoir are small in comparison to the effects of volumetric displacement of lake water (George et al., 2022).

The scenario-based computation of lahar hazards downstream of Mount Rainier by George et al. (2022) may someday be supplanted by Monte Carlo simulations that begin by considering a much broader spectrum of possible lahar

source areas, volumes, and mobilities. Such an approach is indeed feasible for simulations of relatively small debris flows traveling within relatively restricted domains. However, for high-resolution simulations of flow across domains that span many hundreds of square kilometers of rugged terrain, the computation time necessary for a Monte Carlo approach remains very substantial. The lahar simulation illustrated in Figs. 5.14, 5.15, 5.16 and 5.17 used Lidar-derived DEM's with a horizontal resolution as fine as 1 m in some high-consequence areas and used a computational grid resolution refinable to 4 m in all areas. With this high resolution and a computational domain spanning roughly 2500 km<sup>2</sup> (most of which is not shown in Fig. 5.15), some of the individual simulations reported by George et al. (2022) required more than one month of computer run time. This practical limitation will likely decrease as desktop computers become faster and more model users gain access to supercomputers. In the meantime, this limitation highlights the importance of making judicious choices about maximum resolutions used in numerical simulations, as explained in more detail Sect. 5.7 above.

## 5.12 Remaining Challenges and Concluding Advice

Numerical modeling of debris flows has advanced greatly during the past two decades, in part due to increased computational power and availability of DEMs, and in part due to increased sophistication of model equations, numerical solution methods, and model testing. As a result, depth-averaged models of debris flows moving across three-dimensional terrain have reached a state of fruition that enables their useful application to hazard forecasting. Nonetheless, significant challenges remain before debris-flow modeling reaches full maturity and models can be used to forecast hazards with great confidence.

The first and biggest challenge in using numerical models for hazard assessment involves identification of prospective debris-flow

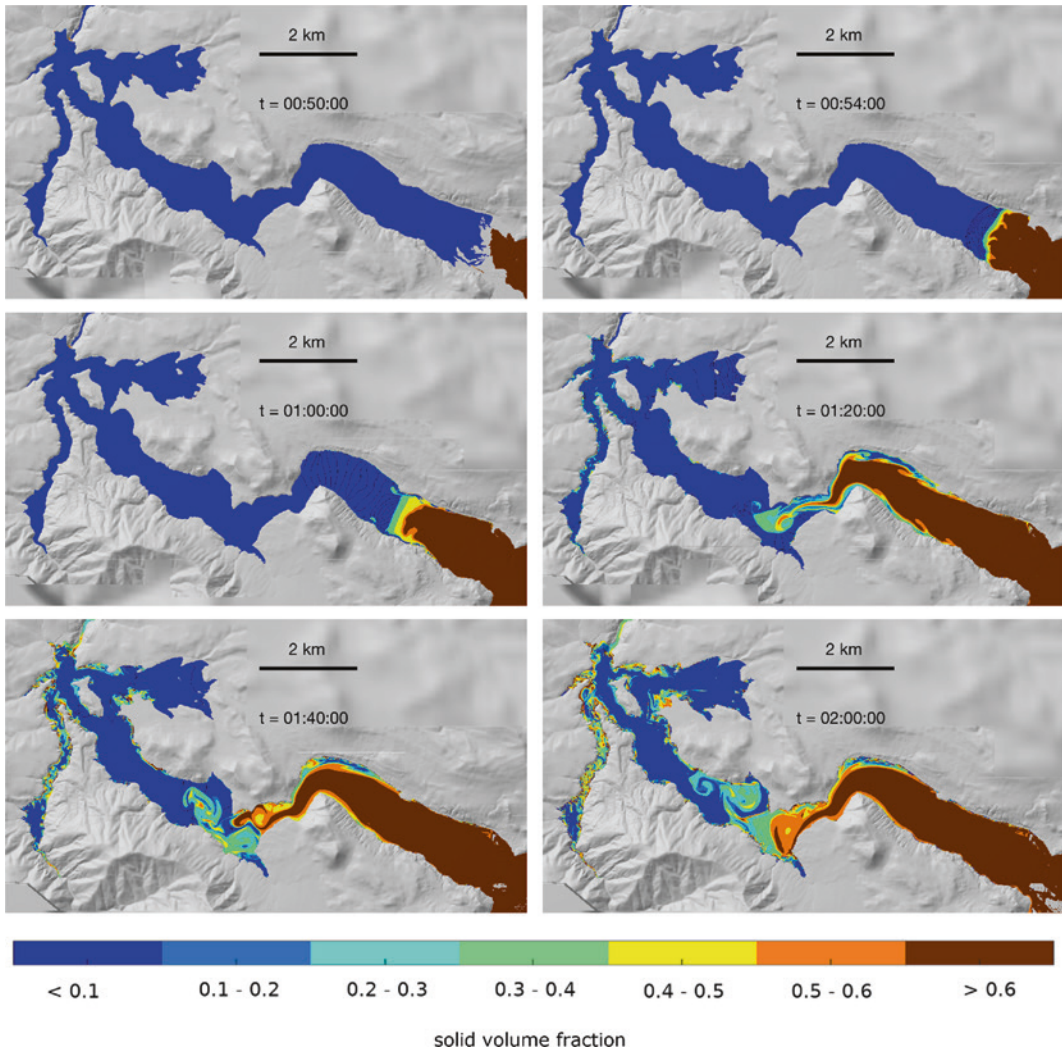


**Fig. 5.17** Time sequence of shaded relief maps showing evolution of solid volume fractions (that is, volumetric sediment concentrations) at selected times as the simulated T-260-HM lahar enters Alder Lake reservoir and mixes with lake water, shown in dark blue

(from George et al., 2022). Time ( $t$ ) is the time elapsed since the onset of landslide/lahar motion, indicated in hours:minutes:seconds. An animated version of the figure is linked to the report of George et al. (2022)

source areas and volumes. Relatively simple, statistically based hazard forecasting models such as Laharz address this problem by considering all plausible source areas and a wide range of flow volumes within a study area (Griswold & Iverson, 2008; Iverson et al., 1998; Reid et al., 2016). However, the computational resources needed to apply Laharz are small in comparison to those required to apply a physically based numerical model such as D-Claw. Thus, in the

foreseeable future, physically based numerical modeling of debris flows will likely focus on relatively limited ranges of possible flow volumes and source areas. This limitation underscores the importance of selecting volumes and source areas based on an a priori assessment of topography and the spatial distribution of debris that can be mobilized. The structure of some numerical models facilitates this process by explicitly considering distributions of potentially unstable,

static debris, whereas other models require information about debris that is assumed to be inherently unstable or already in motion.

A second outstanding challenge, which is related to the first, entails accounting for the effects of debris entrainment or deposition along flow paths. A large body of evidence indicates that entrainment can greatly increase debris-flow volumes and the scope of downstream hazards (e.g., Hungr et al., 2005; Pierson et al., 1990; Reid et al., 2016). Insertion of entrainment terms in depth-averaged debris-flow models is trivial—although appropriate forms of the terms must satisfy mass and momentum conservation constraints identified by Iverson and Ouyang (2015). On the other hand, any entrainment term necessarily includes at least one parameter that cannot be constrained by conservation laws, and accurate computation of entrainment rates that evolve in time and space consequently remains a frontier problem. Large-scale experiments have revealed some key features of the entrainment process (Iverson et al., 2011; Reid et al., 2011), and various models of the process have been suggested (Han et al., 2015), but to our knowledge none have been tested sufficiently to use with great confidence in hazard evaluation.

Another outstanding challenge involves simulating the interrelated processes of grain-size segregation, lateral levee formation, and flow-path avulsion. Grain-size segregation is pervasive in debris flows and commonly leads to formation of boulder-rich lateral levees that help channelize flow downstream (e.g., Fig. 5.3). On the other hand, breaching of levees or overtopping of channels by ensuing debris-flow surges can lead to avulsion and redirection of flow, especially on the divergent topographic surfaces of alluvial fans. Consequently, from a hazards perspective, improved models for forecasting areas of debris-flow inundation should simulate the interrelated processes of grain-size segregation, lateral levee formation, and possible flow-path avulsion. Understanding of the pertinent processes is improving (e.g., Johnson et al., 2012; de Haas et al., 2018), but rigorous inclusion of these processes in physically based models is in its earliest stages.

As we stated in our Introduction, we are model developers ourselves, but we are also model skeptics. All mathematical models of dissipative physical processes such as debris flows are inexact, and all involve tradeoffs between mathematical simplicity and physical realism. In reference to model formulation, Einstein purportedly said that “Everything should be made as simple as possible, but not simpler.” From a practical perspective, debris-flow models aren’t useful if they’re so simple that they omit or misrepresent essential physical phenomena that influence debris-flow hazards. Alternatively, models aren’t useful if they have so many complications that clear links between causes and effects of their predictions aren’t discernible.

Finally, we note that debris-flow models, like debris-flow scientists, provide a benefit to society only insofar as they’re transparent and truthful. Prospective model users should ask questions of models and their developers. Ask about the origin of the model equations—are thorough derivations and explanations of the equations published, or are the equations merely stated? Ask about the model parameters—how are their values determined, and how do they differ for debris flows with various settings and compositions? Ask about the model’s computer source code—is it freely accessible and available for scrutiny? If a model developer makes a bold claim, perhaps that a debris-flow model “simulates entrainment,” ask, “How does it simulate entrainment, and does the method of simulation satisfy physical conservation laws and pass empirical tests?” Finally, it may be appropriate to ask the ultimate question, “If I lived near the path of a simulated future debris flow, would I bet my life on the model’s prediction?”.

---

**Acknowledgements** We thank Charles Cannon for his contributions to the Mount Rainier lahar modeling study summarized in Sect. 5.11 of this paper, and we thank the many USGS colleagues who participated in the debris-flow flume experiments considered in Sects. 5.10.1 and 5.10.2. Oldrich Hungr originally directed our attention to the Mount Meager landslide/lahar event considered in Sect. 5.10.3, and Richard Guthrie and John Clague shared information from their study of the event. Our paper was improved as a result of review comments

provided by Katherine Barnhart, Scott McDougall, Paul Santi, Matthias Jakob, Larry Mastin, and Christopher Magirl. Any use of trade, firm, or product names is for descriptive purposes only and does not imply endorsement by the U.S. Government.

## References

- Allstadt, K. (2013). Extracting source characteristics and dynamics of the August 2010 Mount Meager landslide from broadband seismograms. *Journal of Geophysical Research: Earth Surface*, 118(3), 1472–1490.
- Barnes, N. (2010). Publish your computer code: It is good enough. *Nature*, 467, 753.
- Barnhart, K. R., Jones, R. P., George, D. L., Coe, J. A., & Staley D. M. (2021a). Preliminary assessment of the wave generating potential from landslides at Barry arm, prince William sound, Alaska. U.S. Geol Sur Open-File Report 2021-1071.
- Barnhart, K. R., Jones, R. P., George, D. L., McArdeell, B. W., Rengers, F. K., Staley, D. M., & Kean, J. W. (2021b) Multi-model comparison of computed debris flow runout for the 9 January 2018 Montecito, California post-wild-fire event. *Journal of Geophysical Research: Earth Surface*, 126, e2021JF006245. <https://doi.org/10.1029/2021JF006245>
- Berger, M. J., George, D. L., LeVeque, R. J., & Mandli, K. T. (2011). The GeoClaw software for depth-averaged flows with adaptive refinement. *Advances in Water Resources*, 34(9), 1195–1206. <https://doi.org/10.1016/j.advwatres.2011.02.016>
- Berger, M. J., & Olinger, J. (1984). Adaptive mesh refinement for hyperbolic differential equations. *Journal of Computational Physics*, 53, 484–512.
- Berzi, D., Jenkins, J. T., & Larcher, M. (2010). Debris flows: Recent advances in experiments and modeling. *Advances in Geophysics*, 52, 103–138.
- Bouchut, F. (2004). *Nonlinear stability of finite volume methods for hyperbolic conservation laws and well-balanced schemes for sources*. Birkhauser Verlag.
- Bouchut, F., Fernandez-Nieto, E. D., Mangeney, A., & Narbona-Reina, G. (2016). A two-phase two-layer model for fluidized granular flows with dilatancy effects. *Journal of Fluid Mechanics*, 801, 166–221.
- Bouchut, F., Mangeney-Castelnaud, A., Perthame, B., & Vilotte, J. P. (2003). A new model for Saint Venant and Savage-Hutter type for gravity driven shallow water flows. *Comptes Rendus De L'académie Des Sciences—Series I*, 336, 531–536.
- Breien, H., De Blasio, F. V., Elverhøi, A., & Høeg, K. (2008). Erosion and morphology of a debris flow caused by a glacial lake outburst flood, Western Norway. *Landslides*, 5, 271–280.
- Christen, M., Kowalski, J., & Bartelt, B. (2010). RAMMS: Numerical simulation of dense snow avalanches in three-dimensional terrain. *Cold Regions Science and Technology*, 63, 1–14.
- de Haas, T., Densmore, A. L., Stoffel, M., Suwa, H., Imaizumi, F., Ballesteros-Cánovas, J. A., & Wasklewicz, T. (2018). Avulsions and the spatio-temporal evolution of debris-flow fans. *Earth Science Reviews*, 117, 53–75. <https://doi.org/10.1016/j.earscirev.2017.11.007>
- Denlinger, R. P., & Iverson, R. M. (2004). Granular avalanches across irregular three-dimensional terrain: 1. Theory and computation. *Journal of Geophysical Research: Earth Surface*, 109(F01014). <https://doi.org/10.1029/2003JF000085>
- George, D. L. (2008). Augmented Riemann solvers for the shallow water equations over variable topography with steady states and inundation. *Journal of Computational Physics*, 227(6), 3089–3113.
- George, D. L. (2010). Adaptive finite volume methods with well-balanced Riemann solvers for modeling floods in rugged terrain: Application to the Malpasset dam-break flood (France, 1959). *International Journal for Numerical Methods in Fluids*, 66(8), 1000–1018.
- George, D. L., & Iverson, R. M. (2014). A depth-averaged debris-flow model that includes the effects of evolving dilatancy. II. Numerical predictions and experimental tests. *Proceedings of the Royal Society A: Mathematical, Physical and Engineering Sciences*, 470. <https://doi.org/10.1098/rspa.2013.0820>
- George, D. L., Iverson, R. M., & Cannon, C. M. (2017). New methodology for computing tsunami generation by subaerial landslides: Application to the 2015 Tyndall Glacier landslide, Alaska. *Geophysical Research Letters*, 44(14), 7276–7284.
- George, D. L., Iverson, R. M., & Cannon, C. M. (2022). Modeling the dynamics of lahars that originate as landslides on the west side of Mount Rainier, Washington. U.S. Geol Survey Open-file Report 2021–1118, Reston, Virginia. <https://doi.org/10.3133/ofr20211118>
- George, D. L., & LeVeque, R. J. (2006). Finite volume methods and adaptive refinement for global tsunami propagation and inundation. *Science of Tsunami Hazards*, 24(5), 319–328.
- Godunov, S. K. (1959). A finite difference method for the computation of discontinuous solutions of the equations of fluid dynamics. *Journal of Matematičeskij Sbornik*, 47, 271–306.
- Gray, J. M. N. T., & Kokelaar, B. P. (2010). Large particle segregation, transport and accumulation in granular free-surface flows. *Journal of Fluid Mechanics*, 652, 105–137.
- Gray, J. M. N. T., Tai, Y.-C., & Noelle, S. (2003). Shock waves, dead-zones and particle-free regions in rapid granular free surface flows. *Journal of Fluid Mechanics*, 491, 161–181.
- Gray, J. M. N. T., Wieland, M., & Hutter, K. (1999). Gravity driven free surface flow of granular avalanches over complex basal topography. *Proceedings*

- of the Royal Society of London. Series A, 455, 1841–1874.
- Griswold, J. P., & Iverson, R. M. (2008). Mobility statistics and automated hazard mapping for debris flows and rock avalanches (59 p.). U.S. Geol Sur Sci Invest Rep 2007-5276.
- Guthrie, R. H., Friele, P., Allstadt, K., Roberts, N., Evans, S. G., Delaney, K. B., Roche, D., Clague, J. J., & Jakob, M. (2012). The 6 August 2010 Mount Meager rock slide-debris flow, Coast Mountains, British Columbia: Characteristics, dynamics, and implications for hazard and risk assessment. *Natural Hazards and Earth System Sciences*, 12(5), 1277–1294.
- Han, Z., Chen, G., Li, Y., Tang, C., Xu, L., He, Y., Huang, X., & Wang, W. (2015). Numerical simulation of debris-flow behavior incorporating a dynamic method for estimating the entrainment. *Engineering Geology*, 190, 52–64.
- Hungr, O., Evan, S. G., Bovis, M. J., & Hutchinson, J. N. (2001). A review of the classification of landslides of the flow type. *Environmental and Engineering Geoscience*, 7(3), 221–238.
- Hungr, O., Leroueil, S., & Picarelli, L. (2014). The Varnes classification of landslide types, an update. *Landslides*, 11(2), 167–194.
- Hungr, O., McDougall, S., & Bovis, M. (2005). Entrainment of material by debris flows. In M. Jakob & O. Hungr (Eds.), *Debris flow hazards and related phenomena* (pp. 135–158). Springer-Praxis.
- Iverson, R. M. (1997). The physics of debris flows. *Reviews of Geophysics*, 35, 245–296.
- Iverson, R. M. (2003a). The debris-flow rheology myth. In D. Rickenmann & C. L. Chen (Eds.), *Debris-flow hazards mitigation: Mechanics, prediction, and assessment*, 1 (pp. 303–314). Millpress.
- Iverson, R. M. (2003b). How should mathematical models of geomorphic processes be judged? In P. R. Wilcock & R. M. Iverson (Eds.), *Prediction in geomorphology, geophysical Monograph* (Vol. 135, pp. 83–94). Amer Geophys Union.
- Iverson, R. M. (2005). Debris-flow mechanics. In M. Jakob & O. Hungr (Eds.), *Debris flow hazards and related phenomena* (pp. 105–134). Springer-Praxis.
- Iverson, R. M. (2012). Elementary theory of bed-sediment entrainment by debris flows and avalanches. *Journal of Geophysical Research: Earth Surface*, 117(F03006). <https://doi.org/10.1029/2011JF002189>
- Iverson, R. M. (2015). Scaling and design of landslide and debris-flow experiments. *Geomorphology*, 244, 9–20. <https://doi.org/10.1016/j.geomorph.2015.02.033>
- Iverson, R. M., & George, D. L. (2014). A depth-averaged debris-flow model that includes the effects of evolving dilatancy I. Physical basis. *Proceedings of the Royal Society A: Mathematical, Physical and Engineering Sciences*, 470, 20130819. <https://doi.org/10.1098/rspa.2013.0819>
- Iverson, R. M., & George, D. L. (2016). Modeling landslide liquefaction, mobility bifurcation and the dynamics of the 2014 Oso disaster. *Geotechnique*, 66, 175–187. <https://doi.org/10.1680/jgeot.15.LM.004>
- Iverson, R. M., & George, D. L. (2019a). Basal stress equations for granular debris masses on smooth or discretized slopes. *Journal of Geophysical Research: Earth Surface*, 124, 1464–1484. <https://doi.org/10.1029/2018JF004802>
- Iverson, R. M., & George, D. L. (2019b). Valid debris-flow models must avoid hot starts. In J. W. Kean, J. A. Coe, P. M. Santi, & B. K. Guillen (Eds.), *Debris-flow hazards mitigation: Mechanics, monitoring, modeling, and assessment, Proceedings of the Seventh International Conference on Debris-Flow Hazards Mitigation Monitoring* (Vol. 28, pp. 25–32). Association of Environmental & Engineering Geologists, Special Publication.
- Iverson, R. M., George, D. L., & Logan, M. (2016). Debris flow runup on vertical barriers and adverse slopes. *Journal of Geophysical Research: Earth Surface*, 121, 2333–2357. <https://doi.org/10.1002/2016JF003933>
- Iverson, R. M., George, D. L., Allstadt, K., Reid, M. E., Collins, B. D., Vallance, J. W., Schilling, S. P., Godt, J. W., Cannon, C. M., Magirl, C. S., Baum, R. L., Coe, J. A., Schulz, W. H., & Bower, J. B. (2015). Landslide mobility and hazards: Implications of the 2014 Oso disaster. *Earth and Planetary Science Letters*, 412, 197–208. <https://doi.org/10.1016/j.epsl.2014.12.020>
- Iverson, R. M., Logan, M., LaHusen, R. G., & Berti, M. (2010). The perfect debris flow? Aggregated results from 28 large-scale experiments. *Journal of Geophysical Research: Earth Surface*, 115(F03005). <https://doi.org/10.1029/2009JF001514>
- Iverson, R. M., & Ouyang, C. (2015). Entrainment of bed material by Earth-surface mass flows: Review and reformulation of depth-integrated theory. *Reviews of Geophysics*, 53, 27–58. <https://doi.org/10.1002/2013RG000447>
- Iverson, R. M., Reid, M. E., Iverson, N. R., LaHusen, R. G., Logan, M., Mann, J. E., & Brien, D. L. (2000). Acute sensitivity of landslide rates to initial soil porosity. *Science*, 290, 513–516.
- Iverson, R. M., Reid, M. E., & LaHusen, R. G. (1997). Debris-Flow Mobilization from Landslides. *Annual Review of Earth and Planetary Sciences*, 25, 85–138.
- Iverson, R. M., Reid, M. E., Logan, M., LaHusen, R. G., Godt, J. W., & Griswold, J. G. (2011). Positive feedback and momentum growth during debris-flow entrainment of wet bed sediment. *Nature Geoscience*, 4(2), 116–121. <https://doi.org/10.1038/NNGEO1040>
- Iverson, R. M., Schilling, S. P., & Vallance, J. W. (1998). Objective delineation of lahar-inundation hazard zones. *Geological Society of America Bulletin*, 110, 972–984.

- Johnson, C. G., Kokelaar, B. P., Iverson, R. M., Logan, M., LaHusen, R. G., & Gray, J. M. N. T. (2012). Grain-size segregation and levee formation in geophysical mass flows. *Journal of Geophysical Research*, *117*. <https://doi.org/10.1029/2011JF002185>
- Kowalski, J., & McElwaine, J. N. (2013). Shallow two-component gravity-driven flows with vertical variation. *Journal of Fluid Mechanics*, *714*, 434–462. <https://doi.org/10.1017/jfm.2012.489>
- LeVeque RJ (2002) Finite volume methods for hyperbolic problems. Cambridge University Press.
- LeVeque, R. J. (2013). Top ten reasons to not share your code (and why you should anyway). *SIAM News*, *46*(3), 15.
- LeVeque, R. J., George, D. L., & Berger, M. J. (2011). Tsunami modeling with adaptively refined finite volume methods. *Acta Numerica*, *20*, 211–289. <https://doi.org/10.1017/S0962492911000043>
- Logan, M., Iverson, R. M., & Obyrk, M. K. (2007, revised 2018). Video documentation of experiments at the USGS debris-flow flume, 1992–2017. U.S. Geol Sur Open-file Report 2007-1315. <http://pubs.usgs.gov/of/2007/1315/>
- Lucas, A., Mangeney, A., Bouchut, F., Bristeau, M-O., & Mege, D. (2007). Benchmarking exercises for granular flows. In K. Ho & V. Li (Eds.), *The 2007 International forum on landslide disaster management: Proceedings of the 2007 international forum on landslide disaster management*, Hong Kong, 10–12 December 2007 (pp. 967–986). Geotechnical Division, Hong Kong Institution of Engineers.
- Major, J. J., & Iverson, R. M. (1999). Debris-flow deposition—effects of pore-fluid pressure and friction concentrated at flow margins. *Geological Society of America Bulletin*, *111*, 1424–1434.
- Malvern, L. E. (1969). *Introduction to the mechanics of a continuous medium*. Prentice-Hall.
- Mandli, K. T., Ahmadi, A. J., Berger, M. J., Calhoun, D., George, D. L., Hadimichael, Y., Ketcheson, D. I., Lemoine, G. I., & LeVeque, R. J. (2016). Clawpack: Building an open-source ecosystem for solving hyperbolic PDEs. *PeerJ Computer Science*, *2*, e68.
- McArdell, B. W., Bartlet, P., & Kowalski, J. (2007). Field observations of basal forces and fluid pore pressure in a debris flow. *Geophysical Research Letters*, *34*, L07406. <https://doi.org/10.1029/2006GL029183>
- McCoy, S. W., Kean, J. W., Coe, J. A., Staley, D. M., Wasklewicz, T. A., & Tucker, G. E. (2010). Evolution of a natural debris flow: In situ measurements of flow dynamics, video imagery, and terrestrial laser scanning. *Geology*, *38*, 735–738.
- McCoy, S. W., Kean, J. W., Coe, J. A., Tucker, G. E., Staley, D. M., & Wasklewicz, T. A. (2012). Sediment entrainment by debris flows: In situ measurements from the headwaters of a steep catchment. *Journal of Geophysical Research: Earth Surface*, *117*(F03016). <https://doi.org/10.1029/2011JF002278>
- McDougall, S. (2017). 2014 Canadian Geotechnical Colloquium: Landslide runout analysis—current practice and challenges. *Canadian Geotechnical Journal*, *54*, 605–620. <https://doi.org/10.1139/cgj-2016-0104>
- McDougall, S., & Hungr, O. (2004). A model for the analysis of rapid landslide motion across three-dimensional terrain. *Canadian Geotechnical Journal*, *41*, 1084–1097. <https://doi.org/10.1139/T04-052>
- Mergili, M., Fischer, J.-T., Krenn, J., & Pudasaini, S. P. (2017). R.avaflow v1, an advanced open-source computational framework for the propagation and interaction of two-phase mass flows. *Geoscientific Model Development*, *10*, 553–569. <https://doi.org/10.5194/gmd-10-553-2017>
- Meyrat, G., McArdell, B., Ivanova, K., Müller, C., & Bartelt, P. (2022). A dilatant, two-layer debris flow model validated by flow density measurements at the Swiss illgraben test site. *Landslides*, *19*, 265–276.
- Moretti, L., Allstadt, K., Mangeney, A., Capdeville, Y., Stutzmann, E., & Bouchut, F. (2015). Numerical modeling of the Mount Meager landslide constrained by its force history derived from seismic data. *Journal of Geophysical Research: Solid Earth*, *120*, 2579–2599. <https://doi.org/10.1002/2014JB011426>
- Nessyahu, H., & Tadmor, E. (1990). Non-oscillatory central differencing for hyperbolic conservation laws. *Journal of Computational Physics*, *87*, 408–463.
- O'Brien, J. S., Julien, P. Y., & Fullerton, W. T. (1993). Two-dimensional water flood and mudflow simulation. *Journal of Hydraulic Engineering Division of the American Society of Civil Engineers*, *119*, 244–261.
- Peng, R. D. (2011). Reproducible research in computational science. *Science*, *334*, 1226–1227.
- Peruzzetto, M., Mangeney, A., Bouchut, F., Grandjean, G., Levy, C., Thiery, Y., & Lucas, A. (2021). Topography curvature effects in thin-layer models for gravity-driven flows without bed erosion. *Journal of Geophysical Research: Earth Surface*, *126*, e2020JF005657.
- Pierson, T. C. (1986). Flow behavior of channelized debris flows, Mount St. Helens, Washington. In A. D. Abrahams (Ed.) *Hillslope processes* (pp. 269–296). Allen and Unwin.
- Pierson, T. C., Janda, R. J., Thouret, J. C., & Borrero, C. A. (1990). Perturbation and melting of snow and ice by the 13 November 1985 eruption of Nevado del Ruiz, Colombia, and consequent mobilization, flow and deposition of lahars. *Journal of Volcanology and Geothermal Research*, *41*, 17–66.
- Pitman, E. B., & Le, L. (2005). A two-fluid model for avalanche and debris flows. *Philosophical Transactions of the Royal Society a: Mathematical, Physical and Engineering Sciences*, *363*, 1573–1601. <https://doi.org/10.1098/rsta.2005.1596>

- Pitman, E. B., Nichita, C. C., Patra, A. K., Bauer, A., Sheridan, M., & Bursik, M. (2003). Computing granular avalanches and landslides. *Physics of Fluids*, *15*, 3638–3646.
- Pudasaini, S. P. (2012). A general two-phase debris flow model. *Journal of Geophysical Research: Earth Surface*, *117*(F03010). <https://doi.org/10.1029/2011JF002186>
- Pudasaini, S. P., Wang, Y., & Hutter, K. (2005). Modelling debris flows down general channels. *Natural Hazards and Earth Systems Sciences*, *5*, 799–819. <https://doi.org/10.5194/nhess-5-799-2005>
- Reid, M. E., LaHusen, R. G., & Iverson, R. M. (1997). Debris-flow initiation experiments with diverse hydrologic triggers. In C.-L. Chen (Ed.), *Debris-flow hazards mitigation: Mechanics, prediction, and assessment* (pp. 1–11). American Society of Civil Engineers.
- Reid, M. E., Iverson, R. M., Logan, M., LaHusen, R. G., Godt, J. W., & Griswold, J. G. (2011). Entrainment of bed sediment by debris flows: Results from large-scale experiments. In R. Genevois, D. L. Hamilton, & A. Prestinzi (Eds.), *Fifth international conference on debris-flow hazards mitigation, mechanics, prediction and assessment* (pp. 367–374). Casa Editrice Universita La Sapienza.
- Reid, M. E., Sisson, T. W., & Brien, D. L. (2001). Volcano collapse promoted by hydrothermal alteration and edifice shape, Mount Rainier, Washington. *Geology*, *29*(9), 779–782.
- Reid, M. E., Coe, J. A., & Brien, D. L. (2016). Forecasting inundation from debris flows that grow volumetrically during travel, with application to the Oregon Coast Range, USA. *Geomorphology*, *273*, 396–4011. <https://doi.org/10.1016/j.geomorph.2016.07.039>
- Rickenmann, D., Laigle, D., McArdell, B. W., & Hübl, J. (2006). Comparison of 2D debris-flow simulation models with field events. *Computers & Geosciences*, *10*, 241–264.
- Roberti, G., Ward, B., van Wyk de Vries, B., Friele, P., Perotti, L., Clague, J. J., & Giardino, M. (2018). Precursory slope distress prior to the 2010 Mount Meager landslide, British Columbia. *Landslides*, *15*, 637–647 <https://doi.org/10.1007/s10346-017-0901-0>
- Roberti, G., Friele, P., van Wyk de Vries, B., Ward, B., Clague, J. J., Perotti, L., & Giardino, M. (2017). Rheological evolution of the Mount Meager 2010 debris avalanche, southwestern British Columbia. *Geosphere*, *13*(2), 369–390. <https://doi.org/10.1130/GES01389.1>
- Savage, S. B., & Hutter, K. (1991). The dynamics of avalanches of granular materials from initiation to runout, part I, Analysis. *Acta Mechanica*, *86*, 201–223.
- Scott, K. M., Vallance, J. W., & Pringle, P. T. (1995). Sedimentology, behavior, and hazards of debris flows at Mount Rainier, Washington (56 p.). U.S. Geol Sur Prof Paper 1547.
- Sharp, R. P., & Nobles, L. H. (1953). Mudflow of 1941 at Wrightwood, Southern California. *Geological Society of America Bulletin*, *64*, 647–660.
- Stodden, V., McNutt, M., Bailey, D. H., Deelman, E., Gil, Y., Hanson, B., Heroux, M. A., Ioannidis, J. P. A., & Taufer, M. (2016). Enhancing reproducibility for computational methods. *Science*, *354*, 1240–1241.
- Trujillo-Vela, M. G., Ramos-Cañón, A. M., Escobar-Vargas, J. A., & Galindo-Torres, S. A. (2022). An overview of debris-flow mathematical modeling. *Earth Science Reviews*, *232*, 104135. <https://doi.org/10.1016/j.earscirev.2022.104135>
- Vallance, J. W., & Iverson, R. M. (2015). Lahars and their deposits. In H. Sigurdsson (Ed.), *The encyclopedia of volcanoes* (2nd ed., pp. 649–664). Academic Press. <https://doi.org/10.1016/B978-0-12-385938-9.00037-7>
- Varnes, D. J. (1978). Slope movement types and processes. In R. L. Schuster & R. J. Krizek (Eds.). *Landslides analysis and control* (pp. 11–33). U.S. National Academy of Sciences.
- Vreugdenhil, C. B. (1994). *Numerical methods for shallow-water flow*. Kluwer Academic.